Spatial and temporal evolution of Liassic to Paleocene arc activity in southern Peru unraveled by zircon U-Pb and Hf in-situ data on plutonic rocks

Sophie Demouy, Jean-Louis Paquette, Michel de Saint Blanquat, Mathieu Benoit, E. A. Belousova, Suzanne Y. O'Reilly, Fredy García, Luis C. Tejada, Ricardo Gallegos, Thierry Sempere

Spatial and temporal evolution of Liassic to Paleocene arc activity in southern Peru unraveled by zircon U–Pb and Hf in-situ data on plutonic rocks

Sophie Demouy [a,*], Jean-Louis Paquette [b], Michel de Saint Blanquat [a], Mathieu Benoit [a], Elena A. Belousova [c], Suzanne Y. O'Reilly [c], Fredy García [d], Luis C. Tejada [e], Ricardo Gallegos [e], Thierry Sempere [f]

[a] *Université de Toulouse, GET, Université Paul-Sabatier - CNRS - IRD, 14 avenue Edouard-Belin 31400 Toulouse, France*
[b] *Clermont Université, LMV, Université Blaise Pascal - CNRS - IRD, 5 rue Kessler 63000 Clermont-Ferrand, France*
[c] *Australian Research Council Centre of Excellence for Core to Crust Fluid Systems/GEMOC, Department of Earth & Planetary Sciences, Macquarie University, NSW 2109, Australia*
[d] *Escuela de Ingeniería Geológica, Universidad Nacional de San Agustín, avenida Independencia s/n, Arequipa, Peru*
[e] *Sociedad Minera Cerro Verde S.A.A., Arequipa, Peru*
[f] *ISTerre, Université de Grenoble 1, IRD, CNRS, BP 53, F-38041 Grenoble cedex 9, France*

Cordilleran-type batholiths are built by prolonged arc activity along active continental margins and provide detailed magmatic records of the subduction system evolution. They complement the stratigraphic record from the associated forearcs and backarcs. We performed in-situ U–Pb geochronology and Hf isotope measurements on zircon grains from a large set of plutonic rocks from the Coastal Batholith in southern Peru. This batholith emplaced into the Precambrian basement and the Mesozoic sedimentary cover. We identify two major periods of voluminous arc activity, during the Jurassic (200–175 Ma) and the Late Cretaceous–Paleocene (90–60 Ma). Jurassic arc magmatism mainly resulted in the emplacement of a dominantly mafic suite with ε_{Hf} values ranging from -9.5 to $+0.1$. Published ages south of the Arequipa area suggest that the arc migrated southwestward out of the study area during the Middle Jurassic. After a magmatic gap of 85 Ma, arc activity abruptly resumed 90 Ma ago in Arequipa. Intrusive bodies emplaced into both basement and older Jurassic intrusions and strata. This activity culminated between 70 and 60 Ma with the emplacement of very large volumes of dominantly quartz–dioritic magmas. This last episode may be considered as a flare-up event, characterized by intense magmatic transfers into the crust and rapid relief creation. The Late Cretaceous–Paleocene initial ε_{Hf} are shifted toward positive values (up to $+3.3$ and $+2.6$) compared to the Jurassic ones, indicating either a larger input of juvenile magmas, a lesser interaction with the ancient crust, or an increase of re-melting of young mantle-derived mafic lower crust. These magmatic fluxes with juvenile component are coeval with the onset of the crustal thickening at 90 Ma and represent a significant contribution to the formation of the continental crust in this area.

Keywords:
Andes
Batholith
Flare-up
Crustal growth
Zircon
Ages

1. Introduction

Subduction zones are the only places on Earth where superficial material is re-injected into the deep mantle. The most spectacular consequence of this recycling process is arc magmatism, which represents quantitatively the second largest site of magma formation after ocean ridges, and the main source of continental crust growth (Reymer and Schubert, 1984). This arc magmatism leads to spectacular volcanic activity, as the current circum-pacific 'Ring of Fire', but its main production is represented by the crystallization of intrusive rocks at depth. Only a small proportion of the magma produced in arcs reaches the surface, and the averaged long term volume ratio between intrusive and extrusive igneous rocks in continental arc is estimated to be in the order of 5 or greater (White et al., 2006).

The main geological expression of subduction-related magmatism consists in numerous plutonic bodies that cluster and interfinger to form large linear Cordilleran batholiths below active volcanic arcs (Anderson, 1990; Brown, 1977; Davidson and Arculus, 2006; Dickinson, 2004; Pitcher, 1997). Batholiths record the geologic history of long-term ancient arc activity. Therefore, their study is of key importance to unravel the past geodynamic evolution of subduction systems, from both a petro-geochemical (ages and sources of the magmas, associated crustal growth) and a tectonic (exhumation history, arc migration) point of view.

Recent works have shown that pluton growth in subduction settings is generally spatially and temporally discontinuous (Bartley et al., 2008; Cruden and Mc Caffrey, 2001; Miller et al., 2011; Saint Blanquat, de et al., 2006; Saint Blanquat, de et al., 2011; Vigneresse, 2008), similar to the episodic evolution of volcanic systems (de Silva and Gosnold, 2007; Lipman, 2007). Our understanding of magma transfer in arcs has been improved by the recent new

* Corresponding author. Tel.: +33 561 332 662.
E-mail address: sophie.demouy@get.obs-mip.fr (S. Demouy).

insights on timescales of pluton and batholith emplacement (Coleman et al., 2004; Davis et al., 2011; Gehrels et al., 2009; Leuthold et al., 2012; Matzel et al., 2006; Michel et al., 2008; Miller et al., 2007; Paquette et al., 2003; Walker et al., 2007). These new data have initiated a lively debate on the nature of upper crustal plutonic systems, especially with regard to the link between extrusive and intrusive magmatism and the mechanisms and rate of crustal growth. Continental growth has been shown to be marked by magmatic pulses – or flare-ups – during which magma production may be 2 to 10 times greater than normal background arc activity (de Silva and Gosnold, 2007; DeCelles et al., 2009; Ducea, 2001; Ducea and Barton, 2007; Hawkesworth and Kemp, 2006a; Jicha et al., 2006; Kemp et al., 2006).

The South American Andes has been widely cited as the best example of an ocean–continent collision zone, or active continental margin (Mitchell and Reading, 1969). The western margin of South America is characterized by the occurrence of an elongated linear plutonic belt, the Coastal Batholith. Previous studies have shown that the southern segment of the Coastal Batholith of Peru (Fig. 1) provides a long record of the corresponding arc evolution, from the Jurassic to the Paleogene (Clark et al., 1990; Mukasa, 1986a; Pitcher et al., 1985). However, the precise geological history (>30 Ma) of the regional subduction-related magmatism remains poorly known (Mamani et al., 2010). We focused our study on the Coastal Batholith in the Arequipa area, allowing for a large and almost continuous sampling at the scale of the batholith.

Recent development of in-situ measurements of the U–Pb and Hf isotopes by laser-ablation coupled to plasma-source mass spectrometers provides the possibility to combine U–Pb and Hf analyses on the same zircon grain. The measurement of the Hf isotopic composition on the same grain analyzed for U–Pb analyses ensures that each Hf isotopic measurement is directly linked to a corresponding U–Pb age (e.g., Griffin et al., 2002; Hawkesworth and Kemp, 2006b; Kinny and Maas, 2003; Yang et al., 2007). Because of the high Hf content and the physical resilience of zircon, it has the capacity to efficiently retain isotopic information.

We selected a set of 25 samples from the Coastal Batholith in the Arequipa area. Our target was to (1) precisely document the activity of this paleo-arc section by a systematic geochronological dating of the diverse plutons and (2) provide a first isotopic characterization of magma sources by in-situ analysis of U–Pb and Lu–Hf on zircon.

2. Geological background

In Southern Peru, subduction is active since the beginning of the Paleozoic (570 Ma; Cawood, 2005). Granitic intrusions dated between 468 and 440 Ma constitute the remnants of an Ordovician arc (Fig. 1) (Loewy et al., 2004). A period of magmatic quiescence during the Devonian ends with the emplacement of Carboniferous to Late Triassic plutons around Cuzco (present Eastern Cordillera) from 325 Ma to 215 Ma (Mišković et al., 2009). The Meso-Cenozoic arc activity, during the Liassic to Paleocene period, is the subject of the present study.

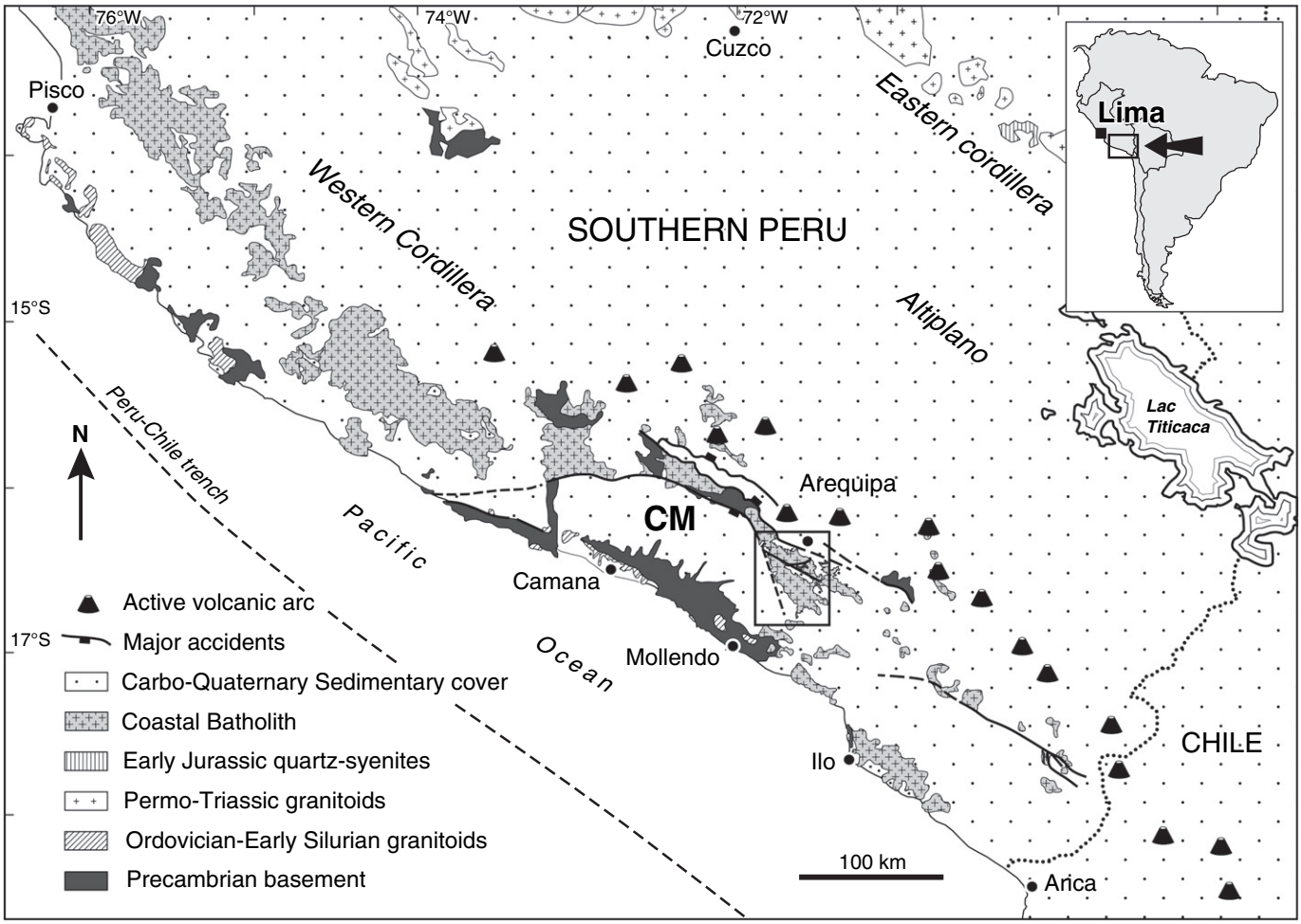

Fig. 1. Simplified map of southern Peru showing the location of the studied area (black square) and the distribution of Ordovician to Mesozoic batholithic rocks. CM: Camaná–Mollendo block.

2.1. Basement

All Proterozoic rocks in the southern part of Peru are collectively grouped under the name "Arequipa massif". They underwent complex, polycyclic magmatic and metamorphic evolution from the Early Proterozoic to the Early Paleozoic. First, a large orogenic cycle between ~2.1 and ~1.8 Ga and then a second main one (Grenvillian event) between 1.2 and 0.97 Ga (Casquet et al. 2010; Loewy et al., 2004). In southern Peru, the Grenvillian event is described in the Camaná–Mollendo block between 1040 and 940 Ma (Casquet et al., 2010; Martignole and Martelat, 2003). These rocks mainly crop out not only along the present-day coastline, where gneisses yield ages of about 1 Ga (Casquet et al., 2010; Loewy et al., 2004), but also in smaller inliers located farther inland, commonly in association with intrusive rocks of the Coastal Batholith (Figs. 1 and 2).

2.2. Volcano-sedimentary cover

The basement is overlain by a thick stratigraphic succession of Late Paleozoic to Neogene age, which consists of volcanoclastic arc products and marine to continental sediments. The Late Paleozoic–Mesozoic part of this succession is about 5 km-thick (Cruz, 2002; Sempere et al., 2002) and is commonly intruded by Jurassic to Paleogene plutons and dikes of various compositions.

2.3. Crustal thickness

The continental crust currently reaches its maximal thickness in the Central Andes below the Central Andean Orocline (CAO, 13°S–28°S). Seismic studies by Beck et al. (1996) and James (1971) estimated the crust to be 70 km thick beneath the Western Cordillera, where little to no shortening is apparent in the upper crust (James, 1971; Kono et al., 1989; Sempere and Jacay, 2008; Sempere et al., 2008). Although past crustal thicknesses are difficult to estimate, geological reconstructions along with geochemical data indicate that crustal thickening slowly started at ~90 Ma and significantly increased by ~30 Ma (Mamani et al., 2010). In contrast, prior to 90 Ma, the Andean crust underwent significant thinning (Sempere et al., 2002).

2.4. The coastal batholith

This batholith forms the core of the Western Cordillera of Peru and is the dominant plutonic feature of the Mesozoic–Paleogene magmatism (Fig. 1). It is composed of more than 1000 plutonic bodies, cropping out over a 1600 km-long and 60 km-wide array, at 150–200 km from the present-day trench. This plutonic belt was formed by the long-lived "subduction factory" along the western margin of North and South America. The present day volcanic arc is located 20 km NE of the batholith, trending NW–SE as defined by the Chachani, El Misti, and Pichu Pichu volcanoes (Fig. 1).

In the Arequipa area, the Coastal Batholith intrudes both the Precambrian basement and the Late Paleozoic to Jurassic sedimentary cover. The plutonic rocks are commonly known as the 'La Caldera' complex or batholith in the literature. The batholith displays a quartz–diorite bulk composition with facies ranging from gabbro to granite (Pitcher et al., 1985). Numerous geochronological studies (K–Ar, Rb–Sr, U–Pb) have been conducted in this area (Beckinsale et al., 1985; Estrada, 1969; Le Bel, 1985; Mukasa, 1986a; Stewart et al., 1974; Cerro Verde S.A.A. proprietary data), concluding that the batholith was mainly assembled between 86 and 53 Ma. Mukasa (1986a) was the first to demonstrate the existence of Jurassic plutons in the northwest and southeast part of the batholith (Fig. 2).

The main structural and petrological dataset on the Peruvian Coastal Batholith was summarized in Pitcher et al. (1985). In our study area, several units were identified (Fig. 2): Incahuasi, Laderas, Gabbros and Diorites, Tiabaya, Linga, and Yarabamba (Le Bel, 1985; Pitcher et al., 1985). They crop out as NW–SE elongated plutonic bodies, the Linga and Yarabamba units being the largest. Structurally, the intrusive rocks are described as nested bell-jar-shaped plutons emplaced by permissive cauldron subsidence and stopping (Pitcher et al., 1985).

3. Field observations and sampling

The studied zone covers an area of 80×60 km out of which about a quarter, i.e. around 1200 km^2, is covered by intrusive rocks (Fig. 2). In the southwestern part of the area, the outcrops provide a continuous 15 km long cross-section of the Linga unit.

3.1. Main results from new mapping

Our mapping (Fig. 2) shows that the Arequipa batholith is divided in two main parts, the northeastern (NEP) and southwest (SWP) parts, separated by the Lluclla fault system (LFS), described to the NW by Sébrier et al. (1985). In the NEP, the batholith is composed of plutons mainly intrusive into the Precambrian basement or older plutons, and corresponds to the Gabbros and Diorites, Laderas, and Tiabaya units of Le Bel (1979). The minimum thickness for the Coastal Batholith in the NEP is around 1 km. In contrast, the SWP is composed of plutons, which were emplaced concordantly within the Jurassic cover, and forms the voluminous Linga unit of Le Bel (1979). The plutons appear to have been tilted about 35° toward the SW after emplacement, as indicated both by the bedding of the sedimentary country rocks and by the geometry of the contacts. This geometry indicates that the minimum thickness of the batholith in the SWP is around 8 km.

Apart from the Mesozoic intrusive rocks, the Lluclla Fault System footwall consists of Precambrian gneiss and their Liassic cover, whereas its hangingwall consists of Middle and Late Jurassic strata (Puente to Labra formations). Toward the southeast, the Yarabamba unit of Le Bel (1979) crops out in both the NEP and SWP, and thus post-dates the activity of the LFS.

Our field observations show that plutons are mainly tabular. Upper and basal sub-concordant pluton–wallrock contacts were observed at several locations throughout the batholith, and the main space-making mechanism appears to have been roof uplift, i.e. upward displacement of wallrocks above the growing pluton.

3.2. Sampling

Sampling was conducted along three transects perpendicular to the main trend of the batholith (Fig. 2) and 25 representative samples were selected for the present study. The location, facies, mineralogy and characteristics of the zircon populations for the dated samples are presented in Table 1, using the unit nomenclature of Le Bel (1979) and Pitcher et al. (1985).

Field observations show that the Gabbros and Diorites unit and the southern part of the Quebrada de Linga are widely intruded by felsic and/or mafic dykes, and are locally affected by ductile deformation and brittle faulting. The plutons from other units are more homogeneous and undeformed, display a magmatic texture, and they locally contain mafic enclaves. Petrological facies range from medium to coarse-grained gabbro to granite. The gabbros display a Cpx–Amph–Plg–Bt mineralogical association. The diorites, quartz–diorites and granites display a common mineralogy (Qz–Plg–Kf–Amph–Bt). Sample locations are shown in Fig. 2.

The transect A, comprises 9 samples (A1 to A9, Table 1) collected along the Uchumayo branch of the Pan American highway over a distance of 20 km. This transect is composed of three main units (Gabbros and Diorites, Tiabaya NW and Linga) cut by the LFS (Fig. 2). The Gabbros and Diorites unit is locally cut by thick (<10 m), E–W-trending, steeply-dipping basaltic and granitic dykes. To the southwest, the Tiabaya NW unit, a 3.5 km-large dioritic pluton

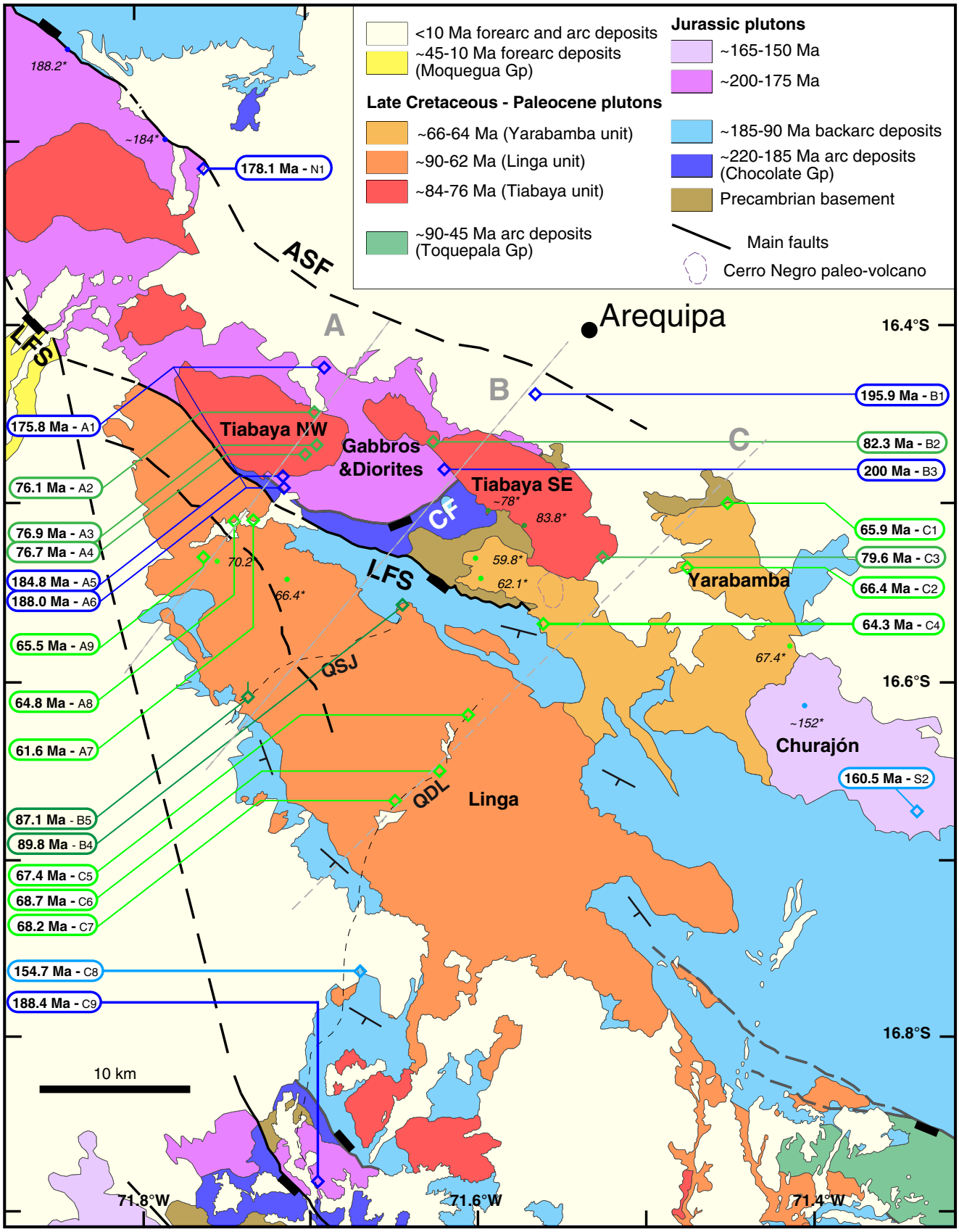

Fig. 2. Geological map of the Arequipa area (this work). LFS: Lluclla Fault System; ASF: Agua Salada Fault; CF: Cenicienta Fault; QSJ: Quebrada San José; QDL: Quebrada de Linga. Thin dotted gray lines indicate the A, B and C transects.

Table 1
Sample descriptions.

Sample	Lat.	Long.	Cross-section	Unit	Facies	Grain size	Mineralogy
09SD27	16° 25.309′S	71° 41.386′W	A1	G&D	Qz–diorite	Medium	Qz–Amph–Plg–Kf–Bt
09SD31	16° 26.812′S	71° 41.516′W	A2	T-NW	Diorite	Medium	Qz–Amph–Plg–Bt–Kf
09SD164	16° 27.928′S	71° 41.669′W	A3	T-NW	Diorite	Coarse	Qz–Amph–Plg–Bt–Kf
09SD35	16° 28.218′S	71° 42.039′W	A4	T-NW	Diorite	Coarse	Qz–Amph–Plg–Bt–Kf
09SD37	16° 28.992′S	71° 42.855′W	A5	G&D	Qz–gabbro	Medium	Qz–Cpx–Amph–Bt
09SD40	16° 29.357′S	71° 42.835′W	A6	G&D	Diorite	Medium	Qz–Amph–Bt–Plg
09SD41	16° 30.473′S	71° 43.951′W	A7	Linga	Diorite	Medium	Qz–Amph–Bt–Plg–Kf
09SD42	16° 30.513′S	71° 44.600′W	A8	Linga	Granite	Coarse	Qz–Kf–Plg–Bt
09SD18	16° 31.737′S	71° 45.727′W	A9	Linga	Qz–diorite	Medium	Qz–Amph–Bt–Plg–Kf
09SD73	16° 26.214′S	71° 33.883′W	B1	G&D	Diorite	Medium	Qz–Amph–Plg–Bt
09SD220	16° 27.863′S	71° 37.533′W	B2	T-SE	Qz–diorite	Coarse	Qz–Amph–Bt–Plg–Kf
09SD221	16° 28.789′S	71° 37.118′W	B3	G&D	Gabbro	Coarse	Plg–CPx–Amph–Sph
09SD131	16° 33.376′S	71° 38.574′W	B4	Linga	Diorite	Medium	Qz–Plg–Bt–Kf
09SD275	16° 36.491′S	71° 44.127′W	B5	Linga	Granite	Medium	Qz–Amph–Bt–Plg–Kf
09SD04	16° 29.970′S	71° 27.101′W	C1	Yar	Diorite	Medium	Qz–Plg–Amph–Bt
09SD109	16° 32.070′S	71° 28.511′W	C2	Yar	Granite	Medium	Qz–Amph–Bt–Plg–Kf
09SD300	16° 31.770′S	71° 31.496′W	C3	T-SE	Qz–diorite	Medium	Qz–Amph–Bt–Plg–Kf
09SD293	16° 34.029′S	71° 33.580′W	C4	Yar	Diorite	Medium	Qz–Amph–Plg–Bt
09SD308	16° 37.114′S	71° 36.278′W	C5	Linga	Diorite	Medium	Qz–Amph–Bt–Plg–Kf
09SD318.A	16° 39.041′S	71° 37.291′W	C6	Linga	Diorite	Medium	Qz–Amph–Bt–Plg–Kf
09SD312	16° 40.037′S	71° 38.917′W	C7	Linga	Diorite	Medium	Qz–Amph–Bt–Plg–Kf
09SD45	16° 45.837′S	71° 40.181′W	C8		Syeno-diorite	Variable	Qz–Plg–Kf–Bt
09SD205	16° 53.094′S	71° 41.778′W	C9		Diorite	Medium	Qz–Px–Amph–Bt
09SD83	16° 18.501′S	71° 45.671′W	N1		Qz–diorite	Coarse	Qz–Amph–Bt–Plg–Kf
09SD331	16° 40.395′S	71° 20.417′W	S1		Diorite	Medium	Qz–Amph–Plg–Bt

Qz = quartz; Plg = plagioclase; Kf = potassic feldspar; Amph = amphibole; Bt = biotite; Cpx = clinopyroxene; Sph = sphène; lat = latitude; long = longitude; G1D = Gabbros and Diorites; T-NW = Tiabaya NW; T-SE = Tiabaya SE; Yar = Yarabamba.

displaying magmatic foliation, crosscuts this unit. Late Neogene ignimbrite deposits cover outcrops between the Gabbros and Diorites unit and the Linga unit. The Linga unit is made of several plutons of massive gabbrodiorite, diorite, quartz diorite and granite displaying magmatic textures and rare evidences of foliation. The transect B comprises 5 samples (B1 to B5, Table 1) that were collected between the southern suburbs of the Arequipa city and the southernmost part of the Quebrada San José, over a distance of 27 km. This transect is made of three units (Gabbros and Diorites, Tiabaya SE and Linga, Fig. 2). The Tiabaya SE unit, a 5.5 km-large pluton, is a homogeneous quartz–diorite that displays large (~3–4 mm) euhedral amphiboles. Transect C is the easternmost and longest section with a length of ~50 km, and comprises 9 samples (C1 to C9, Table 1). This transect consists of three main units (Yarabamba, Tiabaya SE, Linga) and intrusive outcrops located in the southern half part of the Quebrada de Linga. The Yarabamba unit is mostly made of homogeneous quartz–dioritic plutons, associated with sparse gabbrodiorite and granite outcrops. Samples N1 and S1 are located outside the 3 transects but were selected in order to complete our dataset laterally. Sample S1 is a diorite collected close to Churajón. The contact is well exposed and highlights that magma emplacement has produced roof-uplift. Sample N1 is a quartz–diorite collected in the Río Socosani valley, north of the 'La Caldera' complex. This sample displays a clear E–W vertical magmatic foliation, marked by an alignment of ferromagnesian minerals, and is affected by epidote alteration. It is located close to the northeast margin of the batholith that is a faulted contact with recent ignimbrites.

4. Methods

Zircons were separated from the 25 selected samples. Heavy and non-magnetic separates were obtained from the sub-400 μm fraction using standard techniques. Zircon grains between 100 and 300 μm were then handpicked using a binocular microscope and a representative set (including the different morphologies of each sample zircon population) was arranged in rows, cast into one-inch epoxy resin mounts. Minerals were then polished to reveal internal surfaces by cathodoluminescence imaging (CL).

4.1. U–Pb geochronology

The U–Th–Pb geochronology of the zircons was conducted by laser ablation inductively coupled plasma spectrometry (LA-ICPMS) at the Laboratoire Magmas et Volcans, Clermont-Ferrand (France). Analytical conditions are described in detail in Supplementary Table A. The analytical method for isotope dating of zircon with laser ablation ICPMS is reported in Paquette and Tiepolo (2007) and Tiepolo (2003). Concordia ages and diagrams were generated using the Isoplot/Ex v. 2.49 software package by Ludwig (2001). The concentrations in U–Th–Pb were calibrated relative to the certified contents of GJ-1 zircon standard (Jackson et al., 2004). The zircon analyses are projected in $^{207}Pb/^{206}Pb$ versus $^{238}U/^{206}Pb$ diagrams (Tera and Wasserburg 1972), where the analytical points plot along a mixing line between the common Pb composition at the upper intercept and the zircon age at the lower intercept. When common Pb occurs, a linear regression through all analytical points allows calculating a meaningful lower intercept age. In the lack of common Pb, a simple Concordia age is calculated. This is commonly used to date Phanerozoic zircons using in-situ methods (Claoué-Long et al. 1995; Jackson et al. 2004).

4.2. Hf isotope measurements

Measurements were carried out in the Geochemical Analysis Unit of the GEMOC Key Centre in the Department of Earth and Planetary Sciences, Macquarie University, Sydney (Australia). The details of the methodology and analytical conditions for Lu–Hf isotope analysis are provided by Belousova et al. (2009) and Griffin et al. (2000).

Calculation of the ε_{Hf} values was performed using the $\lambda^{176}Lu = 1.865.10^{-11}$ yr^{-1} decay constant of Scherer et al. (2001) as it gives the best fit for terrestrial rocks (Albarède et al., 2006; Amelin and Davis, 2005). We adopted the present CHUR values of Bouvier et al. (2008): $^{176}Lu/^{177}Hf$ (CHUR, today) = 0.0336 and $^{176}Hf/^{177}Hf$ (CHUR, today) = 0.282785. For each analysis, we used the corresponding $^{206}Pb/^{238}U$ age obtained from the LA-ICPMS zircon analyses. T_{DM} model ages were calculated with present day depleted mantle values of $^{176}Lu/^{177}Hf = 0.0384$ (Griffin et al., 2000) and $^{176}Hf/^{177}Hf = 0.28325$ (Griffin et al., 2002), similar to that of the average MORB (Griffin et al., 2004). We assume that the

depleted mantle (DM) reservoir developed from an initially chondritic mantle, and is complementary to the crust extracted over time.

5. Results

5.1. Zircon cathodoluminescence imaging and chemical characteristics

Features of the different zircon populations from each sample are described in Table 2.

Most of the zircon grains have prismatic dipyramidal, euhedral and highly transparent to slightly pink in color. Oscillatory zoning is prominent in the entire zircon population, but some grains display a sector zoning texture (Fig. 3G).

Some of the more mafic samples contain zircon grains with heteromorphic shapes, related to the late reaching of Zr saturation in the crystallization history of the magma (Corfu et al., 2003; Fig. 3B). Zircon grains may incorporate high amounts of incompatible trace elements such as U and Th, which tend to concentrate in the residual melts (both U and Th are reaching values higher than 8000 ppm in 09SD221, cf. Supplementary Table B).

We observe that fine zoning is more marked in the most differentiated facies, related to the long-lived history of the zircons (Fig. 3D and I). Also, zircon textures are more complex, i.e. display more intense zoning features, in the oldest samples compared to the youngest. Paleocene samples display no inherited cores (except for sample 09SD293) and mainly homogeneous crystals (Fig. 3E,F and H), characteristic of autocrystic zircons (Miller et al., 2007).

Xenocrystic cores are subrounded (Fig. 3A and C), and were identified in 7 of the 25 samples. The occurrence of xenocrystic zircon (Miller et al., 2007) as inherited cores is a common feature of many igneous rocks (Corfu et al., 2003).

5.2. U–Pb results

All of the U–Pb zircon data are summarized in Table 2 and detailed analytical data are reported in Supplementary Table B. Locations of all samples can be found in Fig. 2, and U–Pb data are plotted on Fig. 4A,B and C. Uncertainties are given at the 2-sigma level. The detailed results of the inherited cores of the sample 09SD131 and the ages of the entire dataset are represented in relative probability plots in Figs. 5 and 6.

Two main periods of batholith construction in the Arequipa area can be recognized from our U–Pb data. The oldest one took place in the Jurassic ($n=7$), defined by Liassic dates from 200 ± 1.1 Ma (sample 09SD221) down to 175.8 ± 1.2 Ma (09SD27). The empty ellipses that are subconcordant around 165–170 Ma in sample 09SD37 probably result from minor fluid circulations linked to the subsequent emplacement of younger intrusions. The Jurassic activity corresponds to the NW region of the batholith (Laderas and Gabbros and Diorites units), and the southernmost part of Quebrada de Linga (09SD205). The two peripheral samples yield significantly younger dates of 160.5 ± 0.8 Ma for the eastern porphyritic diorite (09SD331), and 154.7 ± 1.0 Ma for a southern syenodiorite sill (09SD45). The empty ellipses around 175 Ma probably result from analysis made with a laser ablation spot located both on inherited core and younger rim.

A Late Cretaceous period of pluton emplacement ($n=7$) is defined by dates ranging from 89.8 ± 0.7 Ma (09SD131) to 76.1 ± 0.4 Ma (09SD31). The two oldest dates are from the SWP and the younger ages are from the NEP, Tiabaya-SE and Tiabaya-NW plutons. This event was closely followed by a period of batholith construction ($n=9$) during the Maastrichtian–Paleocene interval from 68.7 ± 0.5 Ma down to 61.6 ± 0.4 Ma. These ages were obtained in the Linga and Yarabamba units, which are the largest units of the batholith.

Dates obtained on rims and inherited cores vary between Precambrian and Cretaceous–Paleocene, independent of the rock type and the sample location (Table 2). The number of inherited zircons appears to overall decrease with time (Table 2). The two peripheral samples 09SD45 (154.7 ± 1.0 Ma) and 09SD331 (160.5 ± 0.8 Ma) contain zircon grains with inherited cores, and belong to plutonic bodies emplaced in between the main magmatic pulses.

Sample 09SD131 (89.8 ± 0.7 Ma) is the oldest sample of the Late Cretaceous group, and displays a particularly high amount of inherited cores (Table 2). The $^{207}Pb/^{206}Pb$ ages of the inherited cores from this sample (Fig. 5) define two main age peaks at ~1.8 and 1.0 Ga that can

Table 2
Summary of U–Pb data obtained on the Arequipa Batholith.

Sample name	Zircon CL imaging				Geochronological data			
	Size	I.C.	CL texture	Shape	Apparent age			Age range of inherited cores
					n	$^{206}Pb/^{238}U$	2σ	
09SD221	>150 μm	00/27	Osc. Zoning	het.	20	200.0	1.1	
09SD73	>200 μm	00/32	Osc. Zoning	euhed.	20	195.9	1.1	
09SD205	>150 μm	00/32	Osc. Zoning	euhed.	23	188.4	1.0	
09SD40	>150 μm	00/29	Osc. Zoning	euhed.	30	188.0	0.8	
09SD37	>300 μm	00/25	Osc. Zoning	het.	21	184.8	1.0	
09SD83	>250 μm	07/31	Osc. Zoning	euhed.	30	179.1	1.0	Proterozoic
09SD27	>300 μm	04/30	Osc. Zoning	euhed.	25	175.8	1.2	Proterozoic
09SD331	>200 μm	05/35	Osc. Zoning	euhed.	20	160.5	0.8	Paleozoic and Proterozoic
09SD45	>100 μm	05/20	Osc. Zoning	Variable	15	154.7	1.0	Jurassic and Proterozoic
09SD131	>100 μm	29/40	Osc. Zoning	euhed.	11	89.8	0.7	Proterozoic and Archean
09SD275	>150 μm	00/34	Osc. Zoning	euhed.	21	87.1	1.0	
09SD220	>100 μm	00/29	Osc. Zoning	Variable	31	82.3	0.4	
09SD300	>250 μm	00/36	Osc. Zoning	euhed.	20	79.6	0.6	
09SD164	>200 μm	00/31	Osc. Zoning	euhed.	19	76.9	0.6	
09SD35	>200 μm	00/32	Sec. Zoning	euhed.	28	76.7	0.4	
09SD31	>200 μm	05/34	Osc. Zoning	euhed.	38	76.1	0.4	Jurassic
09SD318.a	>300 μm	00/34	Osc. Zoning	euhed.	24	68.7	0.5	
09SD312	>200 μm	00/38	Sec. Zoning	Variable	21	68.2	0.4	
09SD308	>200 μm	00/37	Osc. Zoning	euhed.	18	67.4	0.4	
09SD109	>250 μm	00/30	Osc. Zoning	euhed.	23	66.4	0.4	
09SD04	>200 μm	00/30	Osc. Zoning	euhed.	24	65.9	0.5	
09SD18	>150 μm	00/34	Sec. Zoning	euhed.	32	65.5	0.3	
09SD42	>200 μm	00/32	Sec. Zoning	euhed.	26	64.8	0.4	
09SD293	>100 μm	02/19	Osc. Zoning	Variable	13	64.3	0.5	Proterozoic
09SD41	>150 μm	00/28	Osc. Zoning	euhed.	22	61.6	0.4	

I.C. = number of inherited cores; CL = cathodoluminescence; n = number of analysis of non-inherited cores; euhed. = euhedral; het. = heteromorphic.

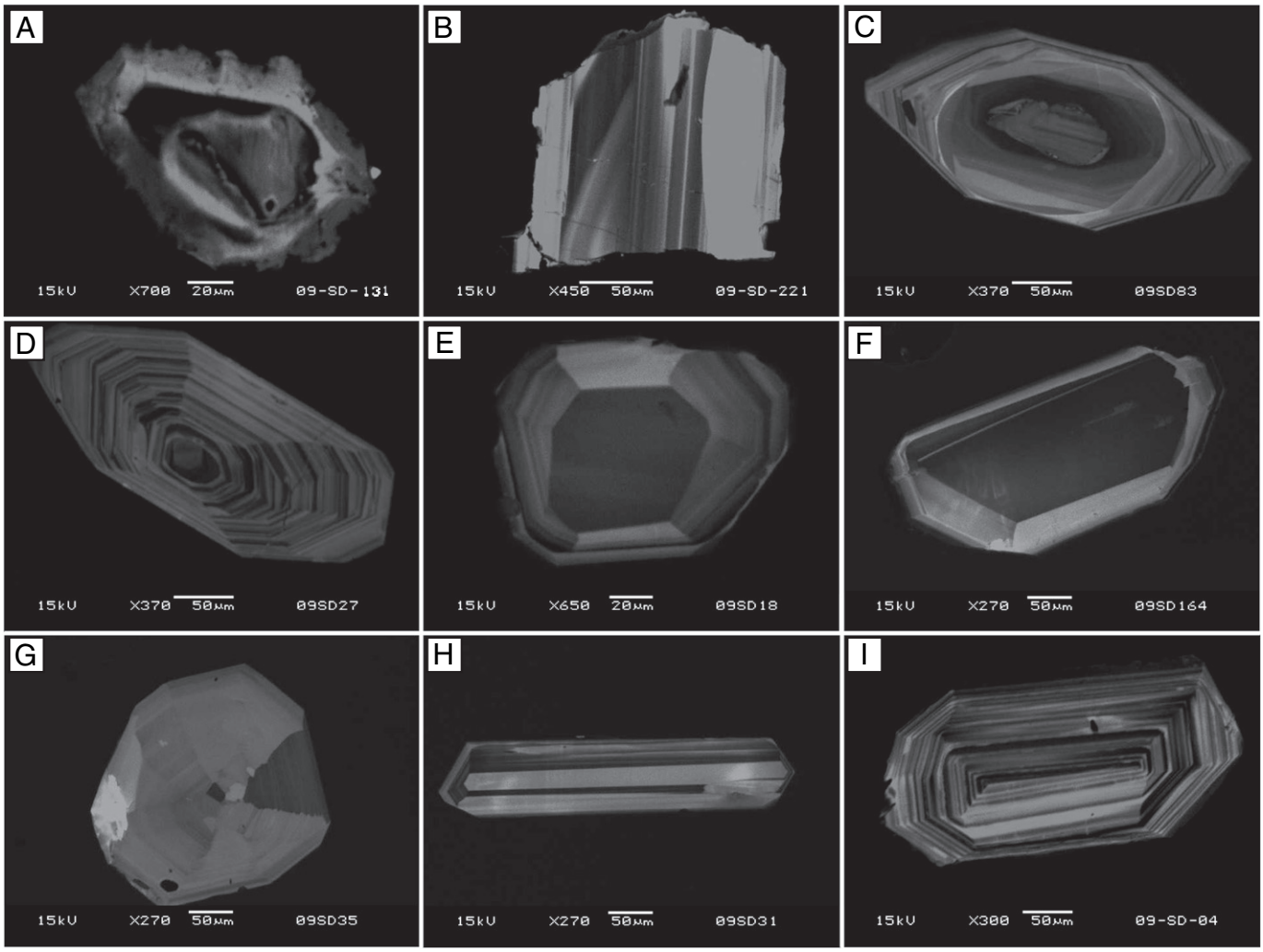

Fig. 3. Zircon CL imaging of selected minerals illustrating the various shapes and structures of analyzed grains. A) 09SD131: Oldest zircon with inherited core dated at 2619 ± 35 Ma. B) 09SD221: typical heteromorphic shape of zircon crystallized in mafic lithologies. C) 09SD83: Proterozoic inherited core surrounded by Jurassic rim. D) 09SD27, E) 09SD18, F) 09SD164, H) 09SD31 and I) 09SD04: typical Cretaceous and Paleocene autocrysts with various oscillatory zoning and no inherited material. G) 09SD37: Jurassic zircon grain with sector zoning texture.

be correlated to two main orogenic cycles that took place in this region (Casquet et al., 2010). Zircon grain 09SD131-005 (Fig. 3) is composed of an inner core surrounded by two growth rims. The inner core yielded a concordant $^{207}Pb/^{206}Pb$ age of 2619 ± 35 Ma, whereas the inner rim yielded a Paleoproterozoic age (~1.8 Ga) and the outer rim a Mesoproterozoic age (~1.1 Ga), both rims being discordant.

5.3. Hf results

14 out of the 25 dated samples were selected for Hf isotope analyses, covering the whole range of U–Pb ages and avoiding inherited cores. Hf data are summarized in Table 3 and reported in a ε_{Hf} vs. time diagram in Fig. 7. Detailed analytical data are reported in Supplementary Table C.

Jurassic magmatic activity is represented by four samples, which yield ε_{Hf} values between −9.5 and +0.1; the inter-sample and intra-sample variabilities are 9.8 and 6.1 ε_{Hf} units respectively. Late Cretaceous intrusions are represented by four samples, which yield ε_{Hf} values ranging from −6.3 to +3.3; the inter-sample and intra-sample variabilities are 10.0 and 4.0 ε_{Hf} units respectively. Maastrichtian–Paleocene intrusions are represented by 6 samples, which yield ε_{Hf} values between −1.6 and +2.6; the inter-sample and intra-sample variabilities are 4.2 and 2.7 ε_{Hf} units, respectively.

In summary, our data show an overall correlation between ε_{Hf} values and U–Pb ages, as well as an increase in ε_{Hf} values and a reduction of inter-sample variability with time. The intra-sample ε_{Hf} variability also decreases with time, and appears to be independent of the number of analyses per sample.

6. Discussion

6.1. New age constraints on the assemblage of the Coastal Batholith

Our dataset shows that the local magmatic arc activity in southern Peru was discontinuous, and occurred in the Arequipa area during two main periods between 200–175 Ma and 90–60 Ma (Fig. 6).

Mukasa (1986a) previously identified Jurassic intrusions only in the northeastern (188 and 184 Ma) and southeastern (~152 Ma) parts of our study area (Fig. 2). Our results show that the Jurassic magmatic activity was spatially more continuous, over a large zone throughout our studied domain, and was constrained between 200 and 175 Ma. Most of the Jurassic plutonic rocks consist of gabbro and diorite emplaced during this period mainly in the NEP but also to a lesser extent in the SWP of the batholith. After this widespread Liassic magmatism, only small volumes of plutonic rocks appear to have been emplaced during the Middle and the Upper Jurassic. The syenodiorite sill sampled in the southern part of the Quebrada de

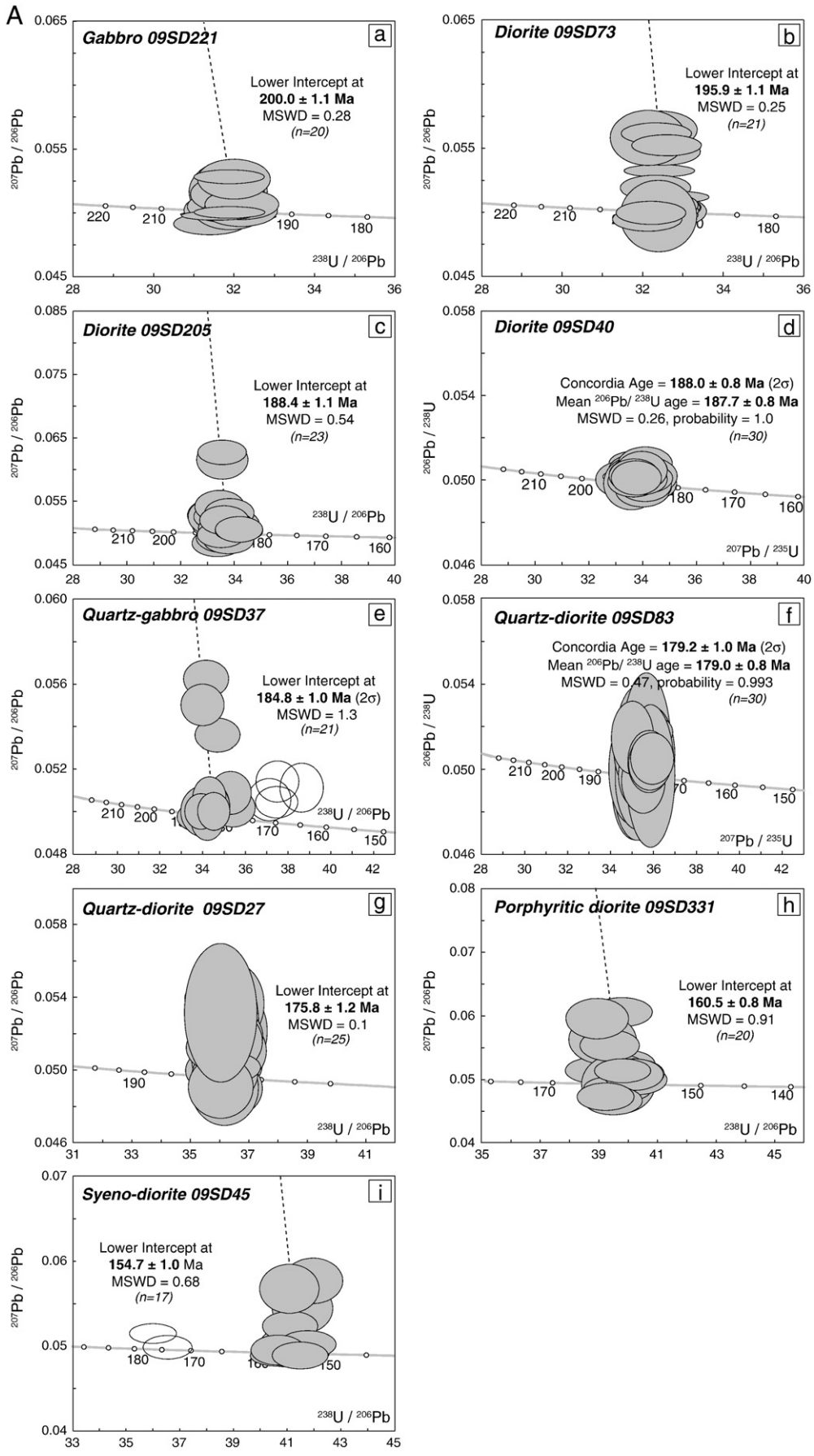

Fig. 4. Concordia plots for plutonic rocks of the Arequipa Batholith dated by LA-ICPMS. All reported errors are 2σ. a) Jurassic range. b) Late Cretaceous range. c) Maastrichtian–Paleocene range. n: number of data.

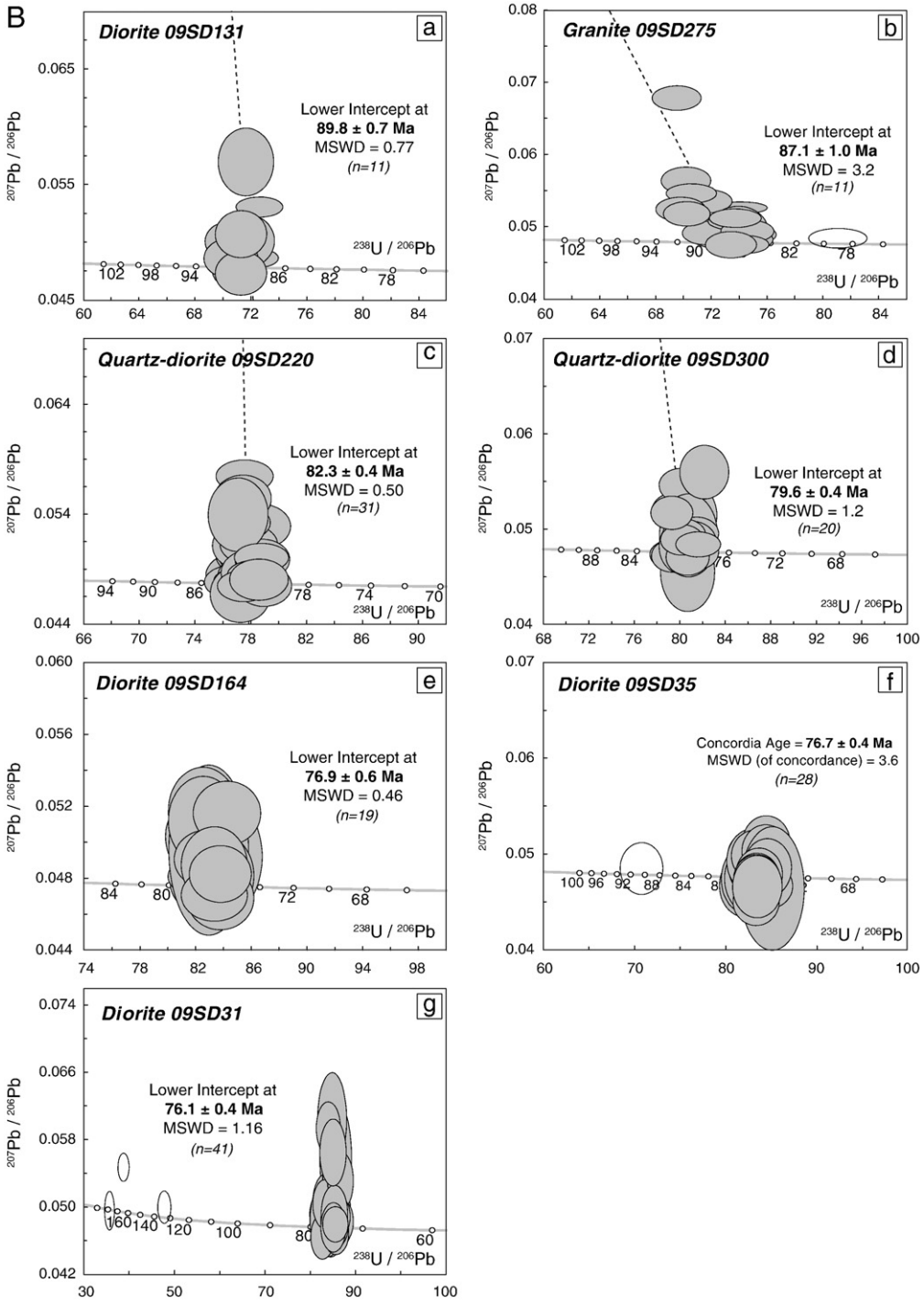

Fig. 4. (*continued*).

Linga (09SD45) yielded a Late Jurassic age of 154.7 ± 1.0 Ma. This sill is part of a rock mélange that most likely represents the local Ayabacas Formation (Thierry Sempéré, pers. com.). This formation is the result of a regional-scale (~100,000 km^2 area of southern Peru), mass-wasting event that occurred at ~90 Ma (Callot et al., 2008). This relationship implies that the sampled rock underwent at least some geographical displacement toward the southwest during the 90 Ma-old Ayabacas collapse (Callot et al., 2008), a point that was unclear at the time of sampling and dating. Consequently, this sample most likely does not indicate the presence of a magmatic activity in its actual location.

No magmatic activity is recorded in the Arequipa area between 160.5 and 90 Ma. The geographic distribution and the density of our sampling strongly suggest that this time gap is real and do not correspond to a sampling artifact.

The onset of Late Cretaceous arc activity (referred as the Toquepala arc; Mamani et al., 2010) is recorded by two ages, at 89.8 ± 0.7 and 87.1 ± 1.0 Ma respectively, obtained in the Quebrada San José (09SD131 and 09SD275). Magmatic activity continued during the Late Cretaceous with the emplacement of the Tiabaya-SE pluton during the ~83–78 Ma interval. The Tiabaya-NW pluton was emplaced at ~77–76 Ma. These two plutons are located in the NEP, and are intruding

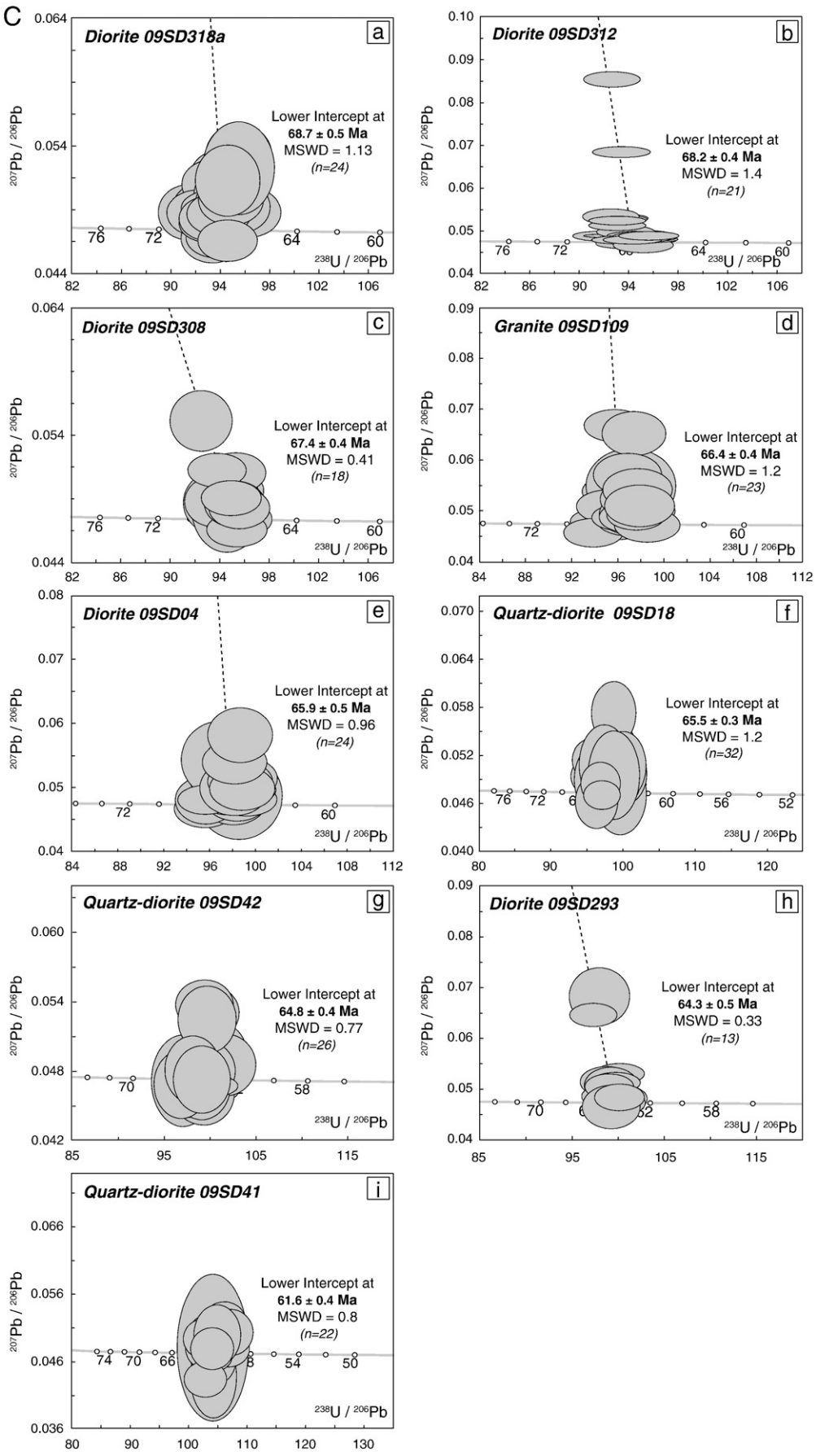

Fig. 4. (*continued*).

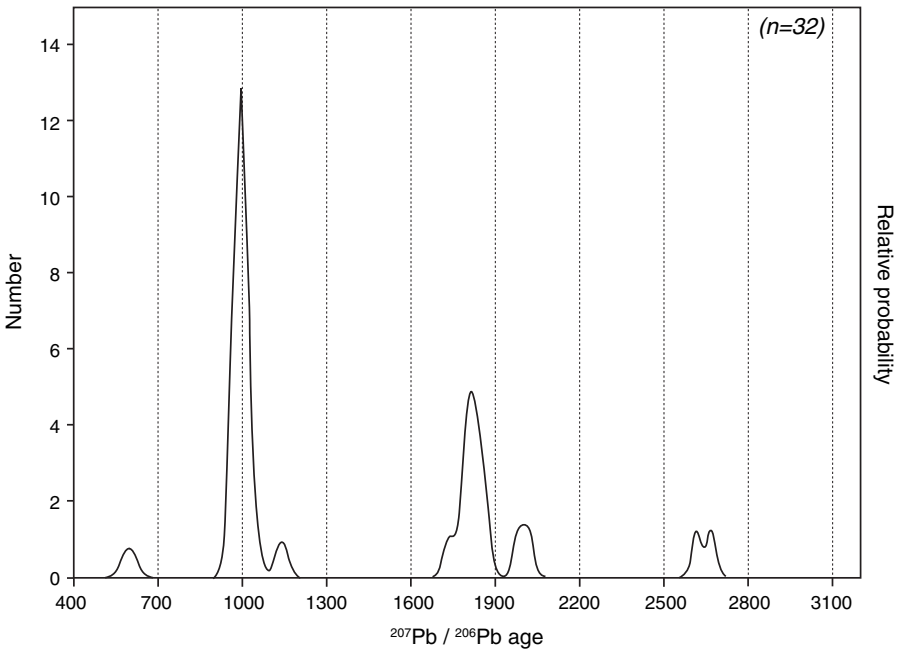

Fig. 5. 09SD131 — Relative probability plot of $^{207}Pb/^{206}Pb$ of inherited cores. The peaks at 2.6 Ga, 1.8 Ga, 1.1 Ga and 600 Ma illustrate the main events that affected the Arequipa basement (Casquet et al., 2010). n: number of data.

mainly into the Liassic component of the batholith, and also locally into the Precambrian basement (Tiabaya-SE only).

After less than 10 Ma of quiescence, the magmatic activity resumes with the emplacement of the most voluminous part of the batholith during the Maastrichtian to Paleocene time interval. The onset of this period is 68.7 ± 0.5 Ma (sample 09SD318a), and was obtained in the northeastern half of the Quebrada de Linga. Plutonic activity is then emplaced across the LFS in the SWP and NEP of the batholith with intrusion between ~66 and ~64 Ma of the NE part of the Linga and of the Yarabamba units. Our youngest U–Pb age is 61.6 ± 0.4 Ma, on a quartz–dioritic sample (09SD41) from the Linga unit and is quite similar to the ages obtained by zircon multigrain U–Pb TIMS analyses in the Cerro Verde mining area (Mukasa, 1986a).

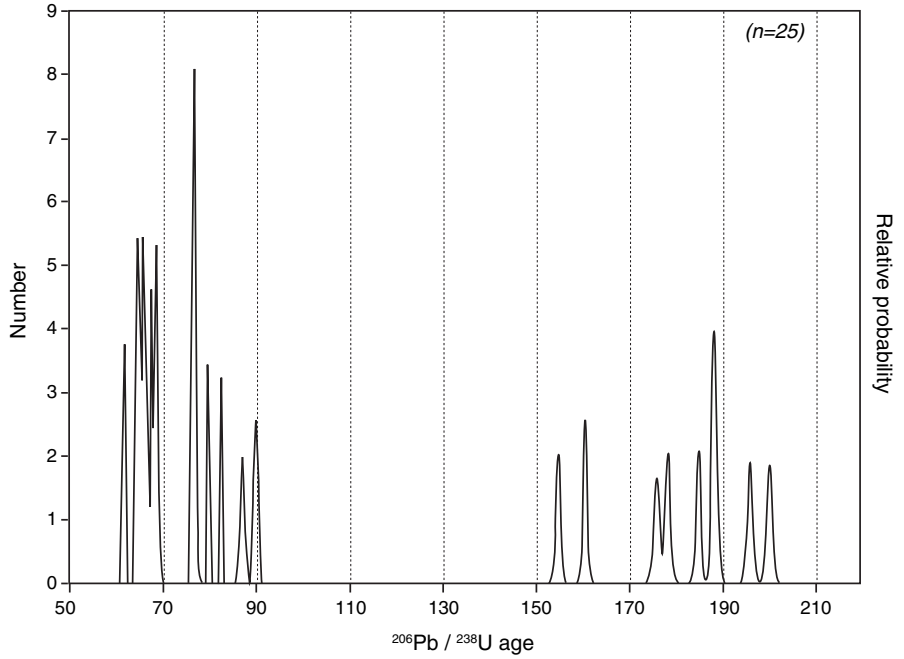

Fig. 6. Relative probability plot of age distribution showing the two main periods of magmatic activity in the Arequipa section of the South Peruvian Coastal Batholith, first between 200 and 175 Ma, and then between 90 and 60 Ma. The 160 and 155 Ma peaks represent the back arc activity of the neighbor Ilo Batholith and an allochthonous sample respectively (see text for more details). n: number of data.

Table 3
Summary of Hf isotopic data obtained on the Arequipa Batholith.

Sample	U–Pb age (Ma)	n	$^{176}Hf/^{177}Hf$ range	1 S.D. $\times 10^6$ range	ε_{Hf} range	1 SE range
09SD221	200.0 ± 1.1	10	0.282596–0.282640	4.9–9.8	−2.5/−0.9	0.2–0.3
09SD40	188.0 ± 0.8	6	0.282631–0.282675	5.7–10	−1.4/+ 0.1	0.2–0.4
09SD27	175.8 ± 1.2	12	0.281557–0.282646	7.3–20	−9.5/−1.2	0.3–0.7
09SD331	160.5 ± 0.8	10	0.282511–0.282607	8.1–13	−6.2/−2.8	0.3–0.5
09SD131	89.8 ± 0.7	7	0.282422–0.282635	7.3–26	−6.3/0.0	0.3–0.9
09SD275	87.7 ± 1.0	16	0.282711–0.282823	6.9–25	−0.8/+ 3.3	0.2–0.9
09SD300	79.6 ± 0.4	13	0.282711–0.282831	6.9–21	−0.8/+ 3.3	0.2–0.7
09SD35	76.7 ± 0.4	11	0.282669–0.282753	8.4–29	−2.5/+ 0.5	0.3–1.0
09SD31	76.1 ± 0.4	10	0.282677–0.282747	7.7–92	−2.3/+ 0.3	0.3–3.3
09SD312	68.2 ± 0.4	13	0.282700–0.282765	7.7–15	−1.6/+ 0.7	0.3–0.5
09SD109	66.4 ± 0.4	13	0.282701–0.282799	8.0–15	−1.5/+ 1.9	0.3–0.5
09SD04	65.9 ± 0.5	12	0.282700–0.282776	7.4–14	−1.6/+ 1.1	0.3–0.5
09SD18	65.5 ± 0.3	15	0.282719–0.282818	9.8–23	−0.9/+ 2.6	0.3–0.8
09SD293	64.3 ± 0.5	10	0.282717–0.282772	6.5–25	−1.0/+ 0.9	0.2–0.9
09SD41	61.6 ± 0.4	16	0.282726–0.282793	7.1–13	−0.7/+ 1.7	0.3–0.5

6.2. Gap in the magmatic activity and arc migration

The synthesis of our U–Pb age distribution is shown in Fig. 6. The most striking feature is that magmatic arc activity in the study area was discontinuous and we can identify a magmatic gap between 175 and 90 Ma, disturbed by only two intermediate samples around 155–161 Ma.

The 154.7 Ma-old sample (09SD45) can be discarded in this case, as it was sampled in a rock mélange, and consequently could not be considered as representative of the Arequipa arc activity at its actual location (see above). The 160.5 Ma-old sample (09SD331) is from the Churajón pluton, near Chapi, in the SE part of our study area. Its emplacement is contemporaneous with the onset of the construction of the Ilo Batholith, which takes place during two pulses between 174 to 152 Ma and 110 to 106 Ma (Boekhout et al., 2012; Clark et al., 1990). The Ilo Batholith comprises the more SE part of the Peruvian Coastal Batholith, and lies >70 km towards the trench, relative to Arequipa. Because of its location (SE part of La Caldera, and in a backarc position with regard to the Ilo Batholith), and of the absence of other intrusions of similar age in our area, the Churajon pluton could be considered as a peripheral back-arc expression of the Ilo arc.

Discontinuous magmatic activity is a common feature in batholiths of South and North America. A major part of the plutonic rocks from central and northern Peru (between 14 and 5°S) were emplaced between 90 and 65 Ma, with some intrusions around 117 and 100 Ma (De Haller et al., 2006; Mukasa, 1986a). In Chile, distinct episodes of pluton emplacement have also been described between 18°S and 56°S. Available data report mostly Jurassic to Early Cretaceous pulses (Dallmeyer et al., 1996; Lucassen et al. 2002; Parada et al., 2005, 2007), and some Late Cretaceous–Paleocene plutons at 22°S (between 79 and 65 Ma, Rogers and Hawkesworth, 1989) and in the South Patagonian Batholith (from 95 to 78 Ma and from 57 to 27 Ma, Herve et al., 2007). In North America, the Sierra Nevada Batholith was constructed by several magmatic pulses, one Jurassic pulse around 160–150 Ma, and a main Cretaceous one between 100 and 85 Ma (Chen and Moore, 1982; Coleman and Glazner, 1997; Ducea, 2001). Thus, even if the ages of magmatic activity are variable along the subduction zone, a general pattern of alternation of magmatic quiescence and plutonic pulses can be found to be a common feature of arc construction. Parada et al. (1988) examined "non-magmatic" intervals and suggested they were related to periods of subduction erosion or

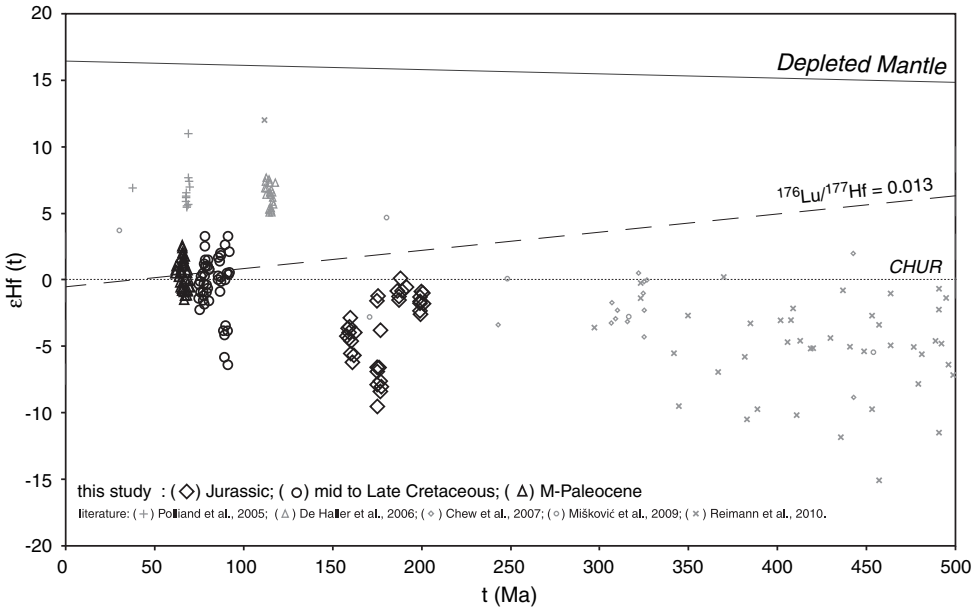

Fig. 7. ε_{Hf} vs U–Pb crystallization ages. The long-dashed line depicts the evolution of a putative crustal reservoir ($^{176}Lu/^{177}Hf = 0013$, Rudnick and Gao, 2005) derived from depleted mantle at 1 Ga. This study: (◊) Jurassic; (○) mid- to Late Cretaceous; (Δ) M–Paleocene. Literature: (+) Polliand et al. (2005); (Δ) De Haller et al. (2006); (◊) Chew et al. (2007); (○) Mišković et al. (2009); (×) Reimann et al. (2010).

changes in dip of the subducted slab. They described 13–16 Myr-long silent intervals in Chile, and a progressive eastward migration of the plutonic belt since the Jurassic. In the Arequipa area, the local magmatic quiescence lasted considerably longer (85 Ma, from 175 to 90 Ma).

Arc migration includes two ways: progressively or by jumps. These events are known to occur in subduction settings. Progressive arc migration implies that the arc position changes with time, as expressed for example by the eastward younging of Cretaceous intrusive rocks in the Sierra Nevada Batholith (Bateman, 1992; Chen and Moore, 1982). Arc jump implies that two areas of arc activity are distinct in time and space, without any geographical connection or the presence of arc rocks displaying intermediate ages. Progressive arc migration thus reflect a gradual variation in slab dip or change in geodynamic setting (e.g. slab roll back), whereas arc jump would have resulted from a more abrupt change in the subduction dynamics. Arc-trench distance and arc-width variations have been related to subduction angle changes (Tatsumi and Eggins, 1995). It has been confirmed that the location of the volcanic arc actually reflects the dynamic of the subducting plate and the associated thermal structure of the slab–mantle wedge system (England and Katz, 2010; England et al., 2004).

The fault-bounded Camaná–Mollendo (CM) block is located in a fore-arc position in respect to the Arequipa arc. It exposes deep crustal levels (Precambrian UHT rocks) and plutons from the Ordovician arc (Casquet et al., 2010; Martignole and Martelat, 2003), and does not present any evidence of Mesozoic arc activity. However, we observe a continuation of the Jurassic arc as evidenced to the south, by the Ilo Batholith (170–160 Ma) intruding partly coeval extrusive Jurassic sequences (Boekhout et al., 2012) along the south Peruvian present-day coastline. To the north of the CM, the extrusive Jurassic arc units have been reported (Chocolate formation dated at 171 and 173 Ma in Chala, 15.9°S, Boekhout-pers comm). This observation might imply that the CM block experienced more exhumation and exhibits a specific geological history.

Consequently, several hypotheses could explain the 85 Ma magmatic gap between 175 and 90 Ma in the Arequipa region, and the absence of magmatism in the fore-arc region of Arequipa where the CM block is located. A first hypothesis is that the arc magmatism remained active and migrated to the CM block. The record was however not preserved, hidden by burial under the recent Cenozoic sedimentary cover or eroded by exhumation of the CM block, exposing the deep crustal levels we now observe at the surface. Another option is that the plutonic record has been removed by subduction erosion, and was originally located just outside the present-day coastline. A third hypothesis is that the arc activity stopped locally, but there is no clear explanation for this event.

The data recently obtained on the Arequipa and Ilo batholiths (Boekhout et al., 2012 and this work) combined with the available geochronological dataset from southern Peru (Clark et al., 1990; Le Bel, 1979), show that the magmatic arc experienced arc migration and possible arc jump events over time (Fig. 8): The Early Jurassic arc (200–175 Ma) extended from the Arequipa area to the southernmost Quebrada de Linga (Fig. 8A). The Middle Jurassic and Early Cretaceous calk-alkaline plutonic rocks that form the Ilo Batholith were emplaced in two main pulses, respectively at ~170–160 Ma and 110–106 Ma, along the present-day coastline (Fig. 8B and D). The existence of a hypothetic 150–110 Ma arc is represented in Fig. 8C. The Late Cretaceous to Paleocene arc (90–55 Ma) was again located in the Arequipa area (Fig. 8E and F). This migration path including first a westward movement and second an eastward movement during the Mesozoic differs from the well-known pattern identified in other Andean segment (e.g. Chilean Coastal Batholith, Patagonian Batholith). In central Chile, the plutonic belts are characterized by eastward decreasing ages (Parada et al., 1988) whereas the locus of the North Patagonian Batholith components does not change significantly with time (Parada et al., 2007).

The Coastal Batholith forms a nearly continuous body northwest of Arequipa, and splits into two branches from this city toward the southeast. Recent geochronological data strongly suggest that these branches reflect different positions of the magmatic arc during distinct periods of arc activity. The northeastern, "inner" branch of the Coastal Batholith, which connects to the Late Cretaceous–Paleocene plutons, was mainly emplaced between 79 and 55 Ma (this work; Beckinsale et al., 1985; Clark et al., 1990). The southwestern, "outer" branch of the batholith was emplaced between ~165 and ~105 Ma, during two main magmatic pulses (Boekhout et al., 2012). There is no evidence that other coeval plutons exist below the Cenozoic cover southwest of Arequipa, forming an extension of this branch toward the northwest. The extrusive equivalent of the Ilo Batholith (the volcanic and volcanoclastic Chocolate Formation) does however extend to the northwest of the CM block.

During the 152–110 Ma magmatic gap observed over the whole south Peruvian margin, several local and global changes occurred. At the south Peruvian scale, the Early Cretaceous marked the end of the extensional context, active since at least Late Permian (Sempere et al., 2002). In the back-arc basin deposits, that are mainly marine from 220 to 90 Ma, the period between 135 and 125 Ma overlaps with the only formation that emplaced in a fluviatile depositional environment (Murco Formation). During this period the arc migration also turned from trenchward to landward. At the South American plate scale, the 135–125 Ma period corresponds to the initiation stages of a significant change in absolute plate motion (Ramos, 2010). From ca. 125 to 100 Ma, the South American continent was practically stationary, before increasing its westward drift after the Cenomanian (Somoza and Zaffarana, 2008). These available data and observations at different scales are consistent with the 135–125 Ma period as a time of major geodynamical change in southern Peru. From 110 Ma onwards, the intrusive rocks recorded the Eastward movement of the arc, first in Ilo (110–106 Ma, Boekhout et al., 2012), then in Arequipa (90–60 Ma, this paper) and then east of Arequipa until 30–24 Ma (Tacaza arc, Mamani et al., 2010).

6.3. Implication for vertical lithospheric movements

From the Permian to the Middle Jurassic, the present Eastern Cordillera and the Arequipa area underwent lithospheric thinning (Sempere et al. 2002). During this period, the arc was located between the Arequipa area and the southernmost Quebrada de Linga. This latter was characterized by a 4500–6000 m-thick sedimentary basin fill sequence, accumulated during lithospheric thinning. The Gabbros and Diorites unit is mainly intrusive into the basement, and provides no clues about its relationships with the sedimentary cover. Near Churajón, sample 09SD331 yields an age of 160.5 ± 0.8 Ma. It comes from a porphyritic diorite that intrudes Jurassic sedimentary strata. These strata display facies of the Cachíos Formation, which is regionally considered of Callovian age on the basis of ammonites belonging to the *Reineckeia* and *Macrocephalites* genera (dated at 164.7 ± 4.0 and 162.8 ± 4.0 Ma, respectively). Mukasa (1986a) already noted a potential discrepancy between the reported Middle to Late Jurassic age of these strata and the 152 Ma-age he obtained on the porphyritic diorite. Our concordant U–Pb age for this diorite of 160.5 ± 0.8 Ma is even closer to the estimated stratigraphic age of the intruded sediments, implying a very short time span between deposition and burial of the sediments and their subsequent intrusion by the diorite. Such a short time span is also documented for the same period in the Ilo Batholith located south of our study area (Boekhout et al., 2012) and strongly suggests that subsidence and deposition rates in the Arequipa backarc basin were very high during the Middle and Late Jurassic.

Evidence of shallow-level magma emplacement is provided by hypovolcanic porphyritic rocks (described as quartz–monzonites) in the Cerro Verde and Santa Rosa porphyry copper deposits. These rocks intruded the Yarabamba quartz–diorite (66.4–64.3 Ma; this study) at 61.0 ± 1.0 Ma (Mukasa, 1986a) and were obviously emplaced at a much shallower depth than the plutonic rocks they intrude, demonstrating that the area underwent rapid exhumation between ~64 and ~61 Ma. This type of rapid denudation of the surface is commonly observed in bulging magmatic arc during flare-up events (DeCelles et

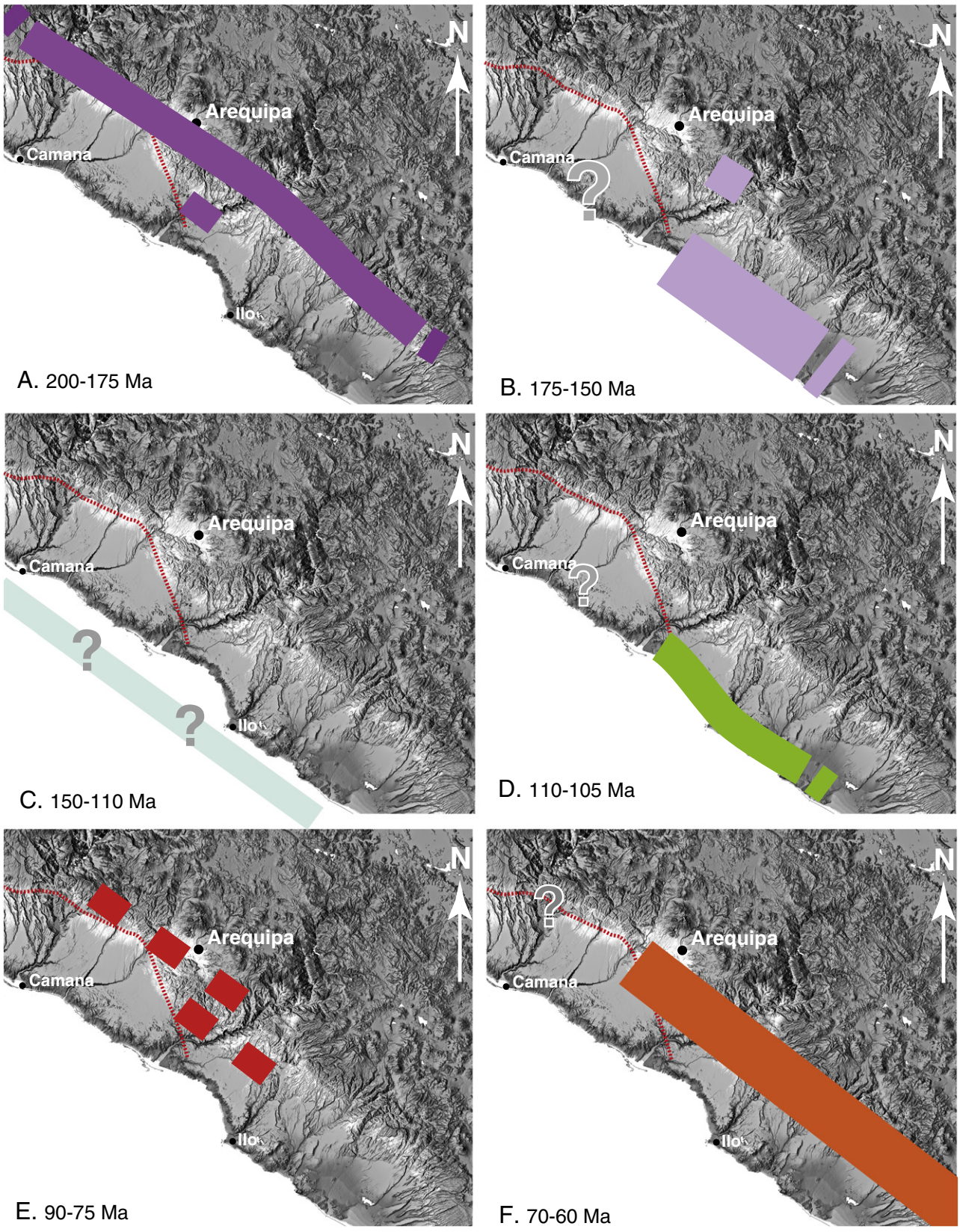

Fig. 8. Migration of the magmatic arc through the southern Peruvian margin from ~200 to 60 Ma, mainly based on available U–Pb data on intrusive rocks (this work; Boekhout et al., 2012; Clark et al. 1990; Mukasa, 1986a). Thin dashed line: limit of the Camaná–Mollendo block. See text for explanations.

al., 2009). Magmatic transfer of hot mass from the mantle thickens the crust beneath the arc. Crustal thickening leads to an enhancement of the relief, which may trigger an increase in erosion rates (provided a stable amount of rainfall) and thus accelerate arc denudation.

6.4. Interpretation of Hf data and implications for crustal growth

Generally, Hf value reflects a mixture of both juvenile and crustal input in different proportions. During the production of magmas, high values of $^{176}Hf/^{177}Hf$ (i.e. $\varepsilon_{Hf}>0$) indicate a dominantly juvenile mantle input, either directly via mantle-derived mafic melts, or by re-melting of young mantle-derived mafic lower crust. Conversely, low values of $^{176}Hf/^{177}Hf$ ($\varepsilon_{Hf}<0$) provide evidence for crustal reworking (Belousova et al., 2006).

Hafnium isotopic signatures from intrusive rocks across the Coastal Batholith in the Arequipa area are much lower than the typical depleted mantle values (ε_{Hf} [500–0 Ma]: +14 to +18, Fig. 7; Vervoort and Blichert-Toft, 1999). This suggests a derivation from crustal sources or very contaminated juvenile mantle melts.

We obtain values between −9.5 and +0.1 for the Jurassic samples (n = 4), −6.3 to +3.3 for the mid-Cretaceous samples (n = 5), and −1.6 to +2.6 for Maastrichtian to Paleocene (M–Paleocene) samples (n = 6). The ranges of ε_{Hf} values are globally decreasing with time. M–Paleocene samples seem to have been derived from magmas that are less heterogeneous than Jurassic and mid-Cretaceous samples. The variation within a single sample (for example > 8 ε_{Hf} units for sample 09SD27) requires open-system processes (Kemp et al., 2007). This implies heterogeneity within and/or among magma sources, possibly related to variable depths of melting (Smith et al. 1987).

The Hf data define two major trends: Jurassic samples show negative ε_{Hf} values which reflect significant crustal input to the melts at this period; Late Cretaceous and Paleocene samples display more elevated ε_{Hf} values, up to +3.3, indicating an increasing amount of juvenile magma in the final arc product. This is in agreement with the smallest amount of inherited cores of the Maastrichtian–Paleocene samples, in comparison with the Jurassic and Cretaceous samples.

At a larger scale, ε_{Hf} values increase with time along the south Peruvian margin since the initiation of the subduction (570 Ma; Cawood, 2005, Fig. 7). The highest ε_{Hf} values along the 12–18°S-Peruvian margin were reported by De Haller et al. (2006) and Polliand et al. (2005) from locations at 60 km ENE and 100 km SE of Lima, respectively. The data above +5 ε_{Hf} values were obtained on Cretaceous–Paleocene plutonic rocks, which are not intrusive into the Precambrian basement but are hosted into a younger, thick sequence of eugeosynclinal volcanics and sediments (Cobbing and Pitcher, 1972). The rocks of the Coastal Batholith at Arequipa emplaced in the Precambrian basement experienced significant crustal contamination, indicated by their crustal ε_{Hf} values, the occurrence of inherited cores of typical basement-ages (this study) and their Pb isotopic signature (Mukasa 1986b). The lower ε_{Hf} isotopic signatures in Arequipa might be related to the different compositions of the assimilated crustal component, or to different rates of crustal contamination.

The nature, i.e. the juvenile vs. crustal ratio, and volumes of the magmatic fluxes constrain the amount of crustal growth (Kemp et al., 2006). Between the Jurassic and the Late Cretaceous–Paleocene events, both parameters differ. First, the Early Jurassic magmatic Hf signature contains smaller amounts of juvenile component. Second, the more mafic composition of the Jurassic magmas supports the idea that they are related to lesser amounts of deep crustal cumulates. To produce igneous rocks that contain more than 60 wt.% SiO_2 by fractional crystallization (like the Late Cretaceous–Paleocene input), 60% or more crystallization of juvenile arc basalt is required (e.g. Foden and Green, 1992; Müntener et al., 2001). This residual mafic volume contributes at this point to the crustal growth process. At the arc scale, we can consider that the 90–60 Ma magmatic activity was a contribution to the production of new crust, on the basis of the positives ε_{Hf} values and the large volumes involved. Future geochemical modeling may help to estimate the respective proportions of mantle (juvenile) and crustal (recycled) inputs.

6.5. A 70–60 Ma flare-up event

Non-steady-state magmatism is a general feature of large-scale granitic magmatism in continental arc areas (Ducea, 2001; Saint Blanquat, de et al., 2011), marked by the alternation of high magmatic flux periods with longer periods of normal "background" activity (de Silva and Gosnold, 2007; Ducea, 2001). For example, in the Mesozoic Sierra Nevada batholith of California, two 10–15-Ma long pulses produced ~78% of the batholitic volume (Ducea, 2001). During high magmatic flux events, the formation of batholith at depth is expressed at the surface by large ignimbritic flare-up (Ducea and Barton, 2007; Hamilton and Myers, 1967; Lipman, 1984). According to the literature, flare-ups can be triggered and driven by catastrophic transient increase in mantle power input (Best and Christiansen, 1991; de Silva et al., 2006a,b; Nieto-Samaniego et al., 1999), or by an increase of the crustal melting (DeCelles et al., 2009).

Figs. 6 and 8 present the estimates of the time and spatial variation of arc activity in southern Peru between the Early Jurassic and the Paleocene. The resulting pattern appears to be comparable with the Sierra Nevada case, in the sense that arc activity mostly occurred in two 25–30-Myr long pulses, one at 200–175 Ma and the other one at 90–60 Ma. Between these two periods, there is no magmatic activity in the area, probably because of arc migration.

In the 90–76 Ma sampled rocks, the oldest Cretaceous age was obtained on a diorite with a relatively high crustal component ($\varepsilon_{Hf}<0$ and many inherited basement zircons; sample 09SD131, Quebrada San José). The second older Cretaceous age was obtained on a granite that displays more juvenile signatures, with ε_{Hf} ranging from −0.8 to +3.3 (sample 09SD275). This suggests that the more crustal characteristics of the ~90 Ma-old magma batch are likely to be related to its earlier emplacement. In the 70–60 Ma sample batch, the ε_{Hf} signatures do not reach such high values but remain globally similar (−1.6 to +2.6) to the ε_{Hf} signatures for the 90–76 Ma period.

This 70–60 Ma plutonic pulse coincided with the eruption of large amounts of ignimbrites as recorded in southern Peru (in the Paralaque Formation, Bellido and Guevara, 1979; Martinez and Cervantes, 2003) and in Bolivia (in the El Molino Formation, Sempere et al., 1997). It seems likely that the Maastrichtian–Danian interval was indeed a time of major magmatic fluxes in this segment of the Andean system, as recorded by both the intrusive and eruptive records at a regional scale.

The thermal state of the crust partly controls how plutons emplace: rising arc magmas progressively heat and soften the crust, allowing for deep accumulation of larger intrusive volumes through time (Annen et al., 2006; de Silva and Gosnold, 2007). The Late Cretaceous magmatic pulse was initiated at ~90 Ma into a portion of upper crust that had cooled since the Late Jurassic. The fact is that ascent and accumulation of large intrusive volumes are difficult in a cold crust; this may explain why the 90–76 Ma-old plutons are smaller and unconnected. In contrast, during the following period, the thermally "receptive" crust promotes accumulation of larger intrusive volumes.

In the North Americans batholiths, the isotopic signatures during flare-ups attest from an increase of the crustal component in magmas (DeCelles et al., 2009; Ducea and Barton, 2007). In Arequipa, the discontinuous record of the magmatic activity keeps us from comparing flare-up events and background magmatic activity during large periods. The period between 90 and 76 Ma could be considered as 'background' magmatic activity in between flare-up periods. The ε_{Hf} values of this period are comprised between −6.5 and +3.3, and display a larger variability than the flare-up (70–60 Ma) signature, with ε_{Hf} values ranging from −1.6 to +2.6. Within the error limits, the highest Hf values are similar for both periods, suggesting a similar nature of the juvenile source of the magmas. The lowest values belong to the Late Cretaceous batch,

due to a stronger crustal contamination especially for sample 09SD131 (ε_{Hf}: −6.3 to −0). The 70–60 Ma period does not record any isotopic pull down. This indicates that the source of the flare-up flux is not dominated by old lower crust reworking as suspected for North American Cordilleras (DeCelles et al., 2009). The flare-up is also triggered by an increase of pluton generation relative to volcanics production. The juvenile component of the magmas comes either from a primitive magma production directly from the mantle or from re-melting of young mantle-derived mafic lower crust. Its increasing amount in the magma composition results from an enhanced production or/and by a decreasing participation of the crust due to its increasing refractory nature with time (Parada et al., 2007).

7. Conclusions

The aim of this paper is to constrain the construction of the Coastal Batholith in the Arequipa area in order to retrieve the dynamic of the Andean magmatic arc activity during the Mesozoic and the beginning of the Cenozoic, i.e. before the onset of major crustal thickening in the area, but during the emergence of proto-Andean relief. We have conducted a systematic geochronological dating of plutons and an isotopic characterization of magma sources by in-situ analysis of U–Pb–Th and Hf on zircon. The main results of our study are the following:

1/ Our new mapping shows that the batholith is divided in two branches, separated by the Lluclla fault system, which was active during batholith construction. Structural sections show that the minimum thickness of this upper crustal batholith is in the order of 8–10 km. The plutons that constitute the batholith are mainly tabular, and the main space-making mechanism appears to have been roof uplift.

2/ The Coastal Batholith along the Arequipa traverse was constructed during two main magmatic pulses, each lasting 25–30 Myr. The first pulse is Jurassic, from 200 to 175 Ma, and corresponds to the 'Chocolate' arc of the literature. It consists mainly in Gabbros and Diorites emplaced throughout our study area. The second and more silicic (diorites to granites) pulse is Late Cretaceous to Paleocene, from 90 to 60 Ma, and corresponds to the 'Toquepala' arc. It could be itself divided in two pulses: the first one with isolated bodies emplaced in the SWP (Linga unit) and the NEP (Tiabaya plutons) of the batholith between 90 and 76 Ma, and the second one with the large plutons (Linga and Yarabamba units) emplaced in the SWP and SEP of the batholith between 68 and 60 Ma. This last pulse constitutes by far the most volumetrically important part of the Coastal Batholith in the Arequipa section.

3/ These two main magma pulses were separated by an 85 Myr-long magmatic gap between 175 and 90 Ma. Regional considerations show that during this period, the arc is first moving trenchward before moving eastward to the Arequipa area. These arc migrations attest from changes of the subduction parameters during the 175–90 Ma period. From ca.135–125 Ma, major changes of the South American plate kinematic could have induced the onset of a northeastern migration of the arc across the southern Peruvian margin.

4/ The amount of juvenile addition to the crust during the construction of the Coastal Batholith varies with time. It is low during the Jurassic, as indicated by negative ε_{Hf} values in zircons. Higher ε_{Hf} values, up to +3.3, in zircons from the Late Cretaceous to Paleocene plutons show an increase of juvenile addition to the crust with decreasing time.

5/ Geological evidences such as large plutonic volumes and important ignimbrites deposits show that the end of the construction of the Coastal Batholith in the Arequipa area corresponds to an important flare-up event, which lasted around 10 Myr around the Cretaceous–Paleocene limit (i.e. the 70–60 Ma period).

6/ The ε_{Hf} isotopic signature of this magmatic flare up, which is similar to the ε_{Hf} isotopic signature of the 90–75 Ma pulse, indicates that the flare-up magma flux is not systematically dominated by the reworking of old lower crust. Consequently, this flare-up could be triggered either by an increase of primitive magma injection directly from the mantle, or by an increase of re-melting of young mantle-derived mafic lower crust.

Supplementary data associated with this article can be found, in the online version, at http://dx.doi.org/10.1016/j.lithos.2012.09.001.

Acknowledgments

The Sociedad Minera Cerro Verde S.A.A has allowed a significant part of the field studies. The project was supported by the IRD (Institut de Recherche pour le Développement) and INSU (Institut National des Sciences de l'Univers-CNRS) SYSTER program. We would like to thank José Berropsi from IRD for the field logistical support in Peru, Mireille Besairie for the mineral separations in LMV (Clermont Ferrand), Norman Pearson for his help during Hf analysis, and Flora Boekhout for her careful rereading. The constructive comments of the two reviewers, M. Poujol and M. Parada, were very useful for the improvement of the manuscript. This is contribution 214 from the ARC Centre of Excellence for Core to Crust Fluid Systems (http://www.ccfs.mq.edu.au) and 852 in the GEMOC Key Centre (http://www.gemoc.mq.edu.au). The Hf analytical data were obtained using instrumentation funded by DEST Systemic Infrastructure Grants, ARC LIEF, NCRIS, industry partners and Macquarie University.

References

Albarède, F., Scherer, E.E., Blichert-Toft, J., Rosing, M., Simionovici, A., Bizzarro, M., 2006. γ-Ray irradiation in the early Solar System and the conundrum of the ^{176}Lu decay constant. Geochimica et Cosmochimica Acta 70, 1261–1270.

Amelin, Y., Davis, W.J., 2005. Geochemical test for branching decay of ^{176}Lu. Geochimica et Cosmochimica Acta 69, 465–473.

Anderson, J.L., 1990. The nature and origin of cordilleran magmatism. Geological Society of America Memoir, 174 (414 pp.).

Annen, C., Blundy, J.D., Sparks, R.S.J., 2006. The genesis of intermediate and silicic magmas in deep crustal hot zones. Journal of Petrology 47, 505–539.

Bartley, J.M., Coleman, D.S., Glazner, A.F., 2008. Incremental pluton emplacement by magmatic crack-seal. Transaction of the Royal Society of Edinburgh: Earth and Environmental Science 97, 383–396.

Bateman, P.C., 1992. Plutonism in the central part of the Sierra Nevada Batholith, California, U.S. Geological Survey Professional Paper, 1483 (186 pp.).

Beck, S.L., Zandt, G., Myers, S.C., Wallace, T.C., Silver, P.G., Drake, L., 1996. Crustal-thickness variations in the central Andes. Geology 24, 407–410.

Beckinsale, R.D., Sanchez-Fernandez, A.W., Brook, M., Cobbing, E.J., Taylor, W.P., Moore, N.D., 1985. Rb–Sr whole-rocks isochron and K–Ar age determinations for the Coastal Batholith of Peru. In: Pitcher, W.S., Atherton, M.P., Cobbing, E.J., Beckinsale, R.D. (Eds.), Magmatism at a Plate Edge, The Peruvian Andes. Blackie (Glasgow) / Halsted Press, New York.

Bellido, E., Guevara, C., 1979. Geología de los Cuadrángulos de Punta Bombón y Clemesi. Carta Geológica Nacional, Lima, p. 92.

Belousova, E.A., Griffin, W.L., O'Reilly, S.Y., 2006. Zircon crystal morphology, trace element signatures and Hf isotope composition as a tool for petrogenetic modelling: examples from Eastern Australian granitoids. Journal of Petrology 47, 329–353.

Belousova, E.A., Reid, A.J., Griffin, W.L., O'Reilly, S.Y., 2009. Rejuvenation vs. recycling of Archean crust in the Gawler Craton, South Australia: evidence from U–Pb and Hf isotopes in detrital zircon. Lithos 113, 570–582.

Best, M.G., Christiansen, E.H., 1991. Limited extension during peak tertiary volcanism, Great Basin of Nevada and Utah. Journal of Geophysical Research 96, 13509–13528.

Boekhout, F., Spikings, R., Sempere, T., Chiaradia, M., Ulianov, A., Schaltegger, U., 2012. Mesozoic arc magmatism along the southern Peruvian margin during Gondwana breakup and dispersal. Lithos 146–147, 48–64.

Bouvier, A., Vervoort, J.D., Patchett, P.J., 2008. The Lu–Hf and Sm–Nd isotopic composition of CHUR: constraints from unequilibrated chondrites and implications for the bulk composition of terrestrial planets. Earth and Planetary Science Letters 273, 48–57.

Brown, G.C., 1977. Mantle origin of Cordilleran granites. Nature 265, 21–24.

Callot, P., Sempere, T., Odonne, F., Robert, E., 2008. Giant submarine collapse of a carbonate platform at the Turonian–Coniacian transition: the Ayabacas Formation, southern Peru. Basin Research 20, 333–357.

Casquet, C., Fanning, C.M., Galindo, C., Pankhurst, R.J., Rapela, C.W., Torres, P., 2010. The Arequipa Massif of Peru: new SHRIMP and isotope constraints on a Paleoproterozoic inlier in the Grenvillian orogen. Journal of South American Earth Sciences 29, 128–142.

Cawood, P.A., 2005. Terra Australis Orogen: Rodinia breakup and development of the Pacific and Iapetus margins of Gondwana during the Neoproterozoic and Paleozoic. Earth-Science Reviews 69, 249–279.

Chen, J.H., Moore, J.G., 1982. Uranium–lead isotopic ages from the Sierra Nevada batholith, California. Journal of Geophysical Research 87 (B6), 4761–4784.
Chew, D.M., Schaltegger, U., Košler, J., Whitehouse, M.J., Gutjahr, M., Spikings, R.A., Mišković, A., 2007. U–Pb geochronologic evidence for the evolution of the Gondwanan margin of the north-central Andes. Geological Society of America Bulletin 119, 697–711.
Claoué-Long, J., Compston, W., Roberts, J., Fanning, C.M., 1995. Two carboniferous ages: a comparison of SHRIMP zircon dating with conventional zircon ages and $^{40}Ar/^{39}Ar$ analysis. In: Berggren, W.A., Kent, D.V., Aubry, M.P., Hardenbol, J. (Eds.), Geochronology, time scales & stratigraphic correlation: SEPM Special Publications.
Clark, A.H., Farrar, E., Kontak, D.J., Langridge, R.J., Arenas F., M.J., France, L.J., McBride, S.L., Woodman, P.L., Wasteneys, H.A., Sandeman, H.A., Archibald, D.A., 1990. Geologic and geochronologic constraints on the metallogenic evolution of the Andes of southeastern Peru. Economic Geology 85, 1520–1583.
Cobbing, E.J., Pitcher, W.S., 1972. The Coastal Batholith of central Peru. Journal of the Geological Society 128, 421–454.
Coleman, D.S., Glazner, A.F., 1997. The Sierra Crest Magmatic Event: rapid formation of juvenile crust during the Late Cretaceous in California. International Geology Review 39, 768–787.
Coleman, D.S., Gray, W., Glazner, A.F., 2004. Rethinking the emplacement and evolution of zoned plutons: geochronologic evidence for incremental assembly of the Tuolumne Intrusive Suite, California. Geology 32, 433–436.
Corfu, F., Hanchar, J.M., Hoskin, P.W.O., Kinny, P., 2003. Atlas of zircon textures. Reviews in Mineralogy and Geochemistry 53, 469–500.
Cruden, A.R., Mc Caffrey, K.J.W., 2001. Growth of plutons by floor subsidence: implications for rates of emplacement, intrusion spacing and melt extraction mechanisms. Physics and Chemistry of the Earth 26, 303–315.
Cruz, M., 2002. Estratigrafia y evolution tectono-sedimentaria de los depositos sinorogenicos del cuadrangulo de Huambo (32-r, Cuadrante-II): Las formaciones Ashua y Huanca. Departamento de Arequipa (PhD thesis). Universidad Nacional San Augustin de Arequipa.
Dallmeyer, R.D., Brown, M., Grocott, J., Graeme, K.T., Treolar, P.J., 1996. Mesozoic magmatic and tectonic events within the Andean plate boundary zone, 26°–27°30′S, North Chile: constraints from $^{40}Ar/^{39}Ar$ mineral ages. Journal of Geology 104, 19–40.
Davidson, J., Arculus, R., 2006. The significance of Phanerozoic arc magmatism in generating continental crust. In: Brown, M., Rushmer, T. (Eds.), Evolution and Differentiation of the Continental Crust. Cambridge University Press, United Kingdom, pp. 135–172.
Davis, J.W., Coleman, D.S., Gracely, J.T., Gaschnig, R., Stearns, M., 2011. Magma accumulation rates and thermal histories of plutons of the Sierra Nevada batholith, California. Contributions to Mineralogy and Petrology 163 (3), 449–465.
De Haller, A., Corfu, F., Fontbote, L., Schaltegger, U., Barra, F., Chiaradia, M., Frank, M., Alvarado, J.Z., 2006. Geology, geochronology, and Hf and Pb isotope data of the Raul-Condestable iron oxide–copper–gold deposit, Central Coast of Peru. Economic Geology 101, 281–310.
de Silva, S.L., Gosnold, W.D., 2007. Episodic construction of batholiths: insights from the spatiotemporal development of an ignimbrite flare-up. Journal of Volcanology and Geothermal Research 167, 320–335.
de Silva, S.L., Zandt, G., Trumbull, R., Viramonte, J., 2006a. Large scale silicic volcanism—the result of thermal maturation of the crust. In: Chen, Y.T. (Ed.), Advances in Geosciences. World Scientific Press.
de Silva, S.L., Zandt, G., Trumbull, R., Viramonte, J., Salas, G., Jimenez, N., 2006b. Large ignimbrite eruptions and volcanotectonic depressions in the Central Andes — a thermomechanical Perspective. In: de Natale, G., Troise, C., Kilburn, C. (Eds.), Mechanisms of activity and unrests at large calderas: Special Publication by Geological Society of London, pp. 47–63.
DeCelles, P.G., Ducea, M., Kapp, P., Zandt, G., 2009. Cyclicity in Cordilleran orogenic systems. Nature Geoscience 2, 251–257.
Dickinson, W.R., 2004. Evolution of the North American Cordillera. Annual Review of Earth and Planetary Sciences 32, 13–45.
Ducea, M., 2001. The California Arc: thick granitic batholiths, eclogitic residues, lithospheric-scale thrusting, and magmatic flare-ups. Geological Society of America Today 11, 4–10.
Ducea, M.N., Barton, M.D., 2007. Igniting flare-up events in Cordilleran arcs. Geology 35, 1047–1050.
England, P.C., Katz, R.F., 2010. Melting above the anhydrous solidus controls the location of volcanic arcs. Nature 467, 700.
England, P., Engdahl, R., Thatcher, W., 2004. Systematic variation in the depths of slabs beneath arc volcanoes. Geophysical Journal International 156, 377–408.
Estrada, F., 1969. Edades radiometricas en las cernanias de Cerro Verde (PhD thesis). Universidad Nacional San Augustin, Arequipa, Peru.
Foden, J.D., Green, D.H., 1992. Possible role of amphibole in the origin of andesite: some experimental and natural evidence. Contributions to Mineralogy and Petrology 109, 479–493.
Gehrels, G., Rusmore, M., Woodsworth, G., Crawford, M., Andronicos, C., Hollister, L., Patchett, J., Ducea, M., Butler, R., Klepeis, K., Davidson, C., Friedman, R., Haggart, J., Mahoney, B., Crawford, W., Pearson, D., Girardi, J., 2009. U–Th–Pb geochronology of the Coast Mountains batholith in north-coastal British Columbia: constraints on age and tectonic evolution. Geological Society of America Bulletin 121, 1341–1361.
Griffin, W.L., Pearson, N.J., Belousova, E., Jackson, S.E., van Achterbergh, E., O'Reilly, S.Y., Shee, S.R., 2000. The Hf isotope composition of cratonic mantle: LA-MC-ICPMS analysis of zircon megacrysts in kimberlites. Geochimica et Cosmochimica Acta 64, 133–147.
Griffin, W.L., Wang, X., Jackson, S.E., Pearson, N.J., O'Reilly, S.Y., Xu, X., Zhou, X., 2002. Zircon chemistry and magma mixing, SE China: in-situ analysis of Hf isotopes, Tonglu and Pingtan igneous complexes. Lithos 61, 237–269.
Griffin, W.L., Belousova, E.A., Shee, S.R., Pearson, N.J., O'Reilly, S.Y., 2004. Archean crustal evolution in the northern Yilgarn Craton: U–Pb and Hf-isotope evidence from detrital zircons. Precambrian Research 131, 231–282.
Hamilton, W., Myers, W.B., 1967. The nature of batholiths. U.S. Geological Survey Professional Paper 544-C, p. 30.
Hawkesworth, C.J., Kemp, A.I.S., 2006a. Evolution of the continental crust. Nature 443, 811–817.
Hawkesworth, C.J., Kemp, A.I.S., 2006b. Using hafnium and oxygen isotopes in zircons to unravel the record of crustal evolution. Chemical Geology 226, 144–162.
Herve, F., Pankhurst, R.J., Fanning, C.M., Calderon, M., Yaxley, G.M., 2007. The South Patagonian batholith: 150 my of granite magmatism on a plate margin. Lithos 97, 373–394.
Jackson, S.E., Pearson, N.J., Griffin, W.L., Belousova, E.A., 2004. The application of laser ablation inductively coupled plasma mass spectrometry to in situ U–Pb zircon geochronology. Chemical Geology 221 (1–2), 47–69.
James, D.E., 1971. Andean crustal and upper mantle structure. Journal of Geophysical Research 76, 3246–3271.
Jicha, B.R., Scholl, D.W., Singer, B.S., et al., 2006. Revised age of Aleutian Island Arc formation implies high rate of magma production. Geology 34 (8), 661–664.
Kemp, A.I.S., Hawkesworth, C.J., Paterson, B.A., Kinny, P.D., 2006. Episodic growth of the Gondwana supercontinent from hafnium and oxygen isotopes in zircon. Nature 439, 580–583.
Kemp, A.I.S., Hawkesworth, C.J., Foster, G.L., Paterson, B.A., Woodhead, J.D., Hergt, J.M., Gray, C.M., Whitehouse, M.J., 2007. Magmatic and crustal differentiation history of granitic rocks from Hf–O isotopes in zircon. Science 315, 980–983.
Kinny, P.D., Maas, R., 2003. Lu–Hf and Sm–Nd isotope systems in zircon. Reviews in Mineralogy and Geochemistry 53, 327–341.
Kono, M., Fukao, Y., Yamamoto, A., 1989. Mountain building in the Central Andes. Journal of Geophysical Research 94, 3891–3905.
Le Bel, F., 1979. Etude des conditions de formation du porphyre cuprifère de Cerro Verde-Santa Rosa (Pérou méridional) pris dans son contexte plutonique (PhD thesis). Université de Lausanne, Switzerland.
Le Bel, L., 1985. Mineralization in the Arequipa segment: the porphyry-Cu deposit of Cerro Verde/Santa Rosa. In: Pitcher, W.S., Atherton, M.P., Cobbing, E.J., Beckinsale, R.D. (Eds.), Magmatism at a Plate Edge, the Peruvian Andes. Blackie Halsted Press, Glasgow and London.
Leuthold, L., Müntener, O., Baumgartner, L., Putlitz, B., Ovtcharova, M., Schaltegger, U., 2012. Time resolved construction of a bimodal laccolith (Torres del Paine, Patagonia). Earth and Planetary Science Letters 325–326, 85–92.
Lipman, P.W., 1984. The roots of ash flow calderas in Western North America: windows into the tops of granitic batholiths. Journal of Geophysical Research 89, 8801–8841.
Lipman, P.W., 2007. Incremental assembly and prolonged consolidation of Cordilleran magma chambers: evidence from the Southern Rocky Mountain volcanic field. Geosphere 3 (1), 42–70.
Loewy, S.L., Connelly, J.N., Dalziel, I.W.D., 2004. An orphaned basement block: the Arequipa–Antofalla Basement of the central Andean margin of South America. Geological Society of America Bulletin 116, 171–187.
Lucassen, F., Escayola, M., Romer, R.L., Viramonte, J., Koch, K., Franz, G., 2002. Isotopic composition of Late Mesozoic basic and ultrabasic rocks from the Andes (23–32°S) — implication for the Andean mantle. Contributions to Mineralogy and Petrology 143, 336–349.
Ludwig, K.R., 2001. User's manual for Isoplot/ex Version 2.49. A Geochronological Toolkit for Microsoft Excel. Berkeley Geochronological Center, Special Publication 1a, Berkeley, USA.
Mamani, M., Worner, G., Sempere, T., 2010. Geochemical variations in igneous rocks of the Central Andean orocline (13°S to 18°S): tracing crustal thickening and magma generation through time and space. Geological Society of America Bulletin 122, 162–182.
Martignole, J., Martelat, J.E., 2003. Regional-scale Grenvillian-age UHT metamorphism in the Mollendo–Camana block (basement of the Peruvian Andes). Journal of Metamorphic Geology 21, 99–120.
Martinez, W., Cervantes, J., 2003. Nuevos datos geocronometricos, geocronometricos, geoquimicos y estructurales entre los paralelos 16° y 18°30′S. Boletines, serie D, 26. Instituto de Geologia Mineria y Metalurgia, Lima, p. 140.
Matzel, J.E.P., Bowring, S.A., Miller, R.B., 2006. Time scales of pluton construction at differing crustal levels: examples from the Mount Stuart and Tenpeak intrusions, North Cascades, Washington. Geological Society of America Bulletin 118, 1412–1430.
Michel, J., Baumgartner, L., Putlitz, B., Schaltegger, U., Ovtcharova, M., 2008. Incremental growth of the Patagonian Torres del Paine laccolith over 90 k.y. Geology 36, 459–462.
Miller, J.S., Matzel, J.E.P., Miller, C.F., Burgess, S.D., Miller, R.B., 2007. Zircon growth and recycling during the assembly of large, composite arc plutons. Journal of Volcanology and Geothermal Research 167, 282–299.
Miller, C.F., Furbish, D.J., Walker, B.A., Claiborne, L.L., Koteas, G.C., Bleick, H.A., Miller, J.S., 2011. Growth of plutons by incremental emplacement of sheets in crystal-rich host: evidence from Miocene intrusions of the Colorado River region, Nevada, USA. Tectonophysics 500, 65–77.
Mišković, A., Spikings, R.A., Chew, D.M., Kosler, J., Ulianov, A., Schaltegger, U., 2009. Tectonomagmatic evolution of Western Amazonia: geochemical characterization and zircon U–Pb geochronologic constraints from the Peruvian Eastern Cordilleran granitoids. Geological Society of America Bulletin 121, 1298–1324.
Mitchell, A.H., Reading, H.G., 1969. Continental margins, geosynclines, and ocean floor spreading. Journal of Geology 77 (6), 629–646.
Mukasa, S.B., 1986a. Zircon U–Pb ages of super-units in the Coastal batholith, Peru: implications for magmatic and tectonic processes. Geological Society of America Bulletin 97, 241–254.

Mukasa, S.B., 1986b. Common Pb isotopic compositions of the Lima, Arequipa and Toquepala segments in the Coastal batholith, Peru: implications for magmagenesis. Geochimica et Cosmochimica Acta 50, 771–782.
Müntener, O., Kelemen, P., Grove, T., 2001. The role of H_2O during crystallization of primitive arc magmas under uppermost mantle conditions and genesis of igneous pyroxenites: an experimental study. Contributions to Mineralogy and Petrology 141, 643–658.
Nieto-Samaniego, A.F., Ferrari, L., Alaniz-Alvarez, S.A., Labarthe-Hernandez, G., Rosas-Elguera, J., 1999. Variation of Cenozoic extension and volcanism across the southern Sierra Madre Occidental volcanic province, Mexico. Geological Society of America Bulletin 111, 347–363.
Paquette, J.L., Tiepolo, M., 2007. High resolution (5 μm) U–Th–Pb isotope dating of monazite with excimer laser ablation (ELA)-ICPMS. Chemical Geology 240, 222–237.
Paquette, J.L., Ménot, R.P., Pin, C., Orsini, J.B., 2003. Episodic and short-lived granitic pulses in a post-collisional setting: evidence from precise U–Pb zircon dating through a crustal cross-section in Corsica. Chemical Geology 198, 1–20.
Parada, M.A., Rivano, S., Sepulveda, P., Herve, M., Herve, F., Puig, A., Munizaga, F., Brook, M., Pankhurst, R.J., Snelling, N., 1988. Mesozoic and Cenozoic plutonic development in the Andes of central Chile (30°30′–32°30′S). Journal of South American Earth Sciences 1, 249–260.
Parada, M.A., Féraud, G., Fuentes, F., Aguirre, L., Morata, D., Larrondo, P., 2005. Ages and cooling history of the Early Cretaceous Caleu pluton: testimony of a switch from a rifted to a compressional continental margin in central Chile. Journal of the Geological Society of London 162, 273–287.
Parada, M.A., López-Escobar, L., Oliveros, V., Fuentes, F., Morata, D., et al., 2007. Andean magmatism. In: Moreno, T., Gibson, W. (Eds.), The Geology of Chile. The Geological Society of London, pp. 115–146.
Pitcher, W.S., 1997. The Nature and Origin of Granite. Chapman & Hall . (387 pp.).
Pitcher, W.S., Atherton, M.P., Cobbing, E.J., Beckinsale, R.D. (Eds.), 1985. Magmatism at a Plate Edge, the Peruvian Andes. Blackie (Glasgow) / Halsted Press, New York.
Polliand, M., Schaltegger, U., Frank, M., Fontboté, L., 2005. Formation of intra-arc volcanosedimentary basins in the western flank of the central Peruvian Andes during Late Cretaceous oblique subduction: field evidence and constraints from U–Pb ages and Hf isotopes. International Journal of Earth Sciences 94, 231–242.
Ramos, V.A., 2010. The tectonic regime along the Andes: present-day and Mesozoic regimes. Geological Journal 45, 2–25.
Reimann, C.R., Bahlburg, H., Kooijman, E., Berndt, J., Gerdes, A., Carlotto, V., Lopez, S., 2010. Geodynamic evolution of the early Paleozoic Western Gondwana margin 14°–17°S reflected by the detritus of the Devonian and Ordovician basins of southern Peru and northern Bolivia. Gondwana Research 18, 370–384.
Reymer, A., Schubert, G., 1984. Phanerozoic addiction rates to the continental crust and crustal growth. Tectonics 3, 63–67.
Rogers, G., Hawkesworth, C.J., 1989. A geochemical traverse across the North Chilean Andes: evidence for crust generation from the mantle wedge. Earth and Planetary Science Letters 91, 271–285.
Rudnick, R.L., Gao, S., 2005. Composition of the continental crust. In: Rudnick, R.L. (Ed.), The Crust. Elsevier-Pergamon, Oxford.
Saint Blanquat (de), M., Habert, G., Horsman, E., Morgan, S.S., Tikoff, B., Launeau, P., Gleizes, G., 2006. Mechanisms and duration of non-tectonically assisted magma emplacement in the upper crust: the Black Mesa pluton, Henry Mountains, Utah. Tectonophysics 428, 1–31.
Saint Blanquat (de), M., Horsman, E., Habert, G., Morgan, S., Vanderhaeghe, O., Law, R., Tikoff, B., 2011. Multiscale magmatic cyclicity, duration of pluton construction, and the paradoxical relationship between tectonism and plutonism in continental arcs. Tectonophysics 500, 20–33.
Scherer, E., Munker, C., Mezger, K., 2001. Calibration of the lutetium–hafnium clock. Science 293 (5530), 683–687.
Sébrier, M., Mercier, J.L., Mégard, F., Laubacher, G., Carey-Gailhardis, E., 1985. Quaternary normal and reverse faulting and the state of stress in the Central Andes of South Peru. Tectonics 4, 739–780.
Sempere, T., Jacay, J., 2008. Anatomy of the central Andes: distinguishing between western, magmatic Andes and eastern, tectonic Andes. Extended Abstract, 7th International Symposium on Andean Geodynamics, Nice, pp. 504–507.
Sempere, T., Butler, R.F., Richards, D.R., Marshall, L.G., Sharp, W., Swisher, C.C., 1997. Stratigraphy and chronology of Upper Cretaceous–lower Paleogene strata in Bolivia and northwest Argentina. Geological Society of America Bulletin 109, 709–727.
Sempere, T., Carlier, G., Soler, P., Fornari, M., Carlotto, V., Jacay, J., 2002. Late Permian–Middle Jurassic lithospheric thinning in Peru and Bolivia, and its bearing on Andean-age tectonics. Tectonophysics 345, 153–181.
Sempere, T., Folguera, A., Gerbault, M., 2008. New insights into Andean evolution: an introduction to contributions from the 6th ISAG symposium (Barcelona, 2005). Tectonophysics 459, 1–13.
Smith, P.E., Tatsumoto, M., Farquhar, R.M., 1987. Zircon Lu–Hf systematics and the evolution of the Archean crust in the southern Superior Province, Canada. Contributions to Mineralogy and Petrology 97, 93–104.
Somoza, R., Zaffarana, C.B., 2008. Mid-Cretaceous polar standstill of South America, motion of the Atlantic hotspots and the birth of the Andean cordillera. Earth and Planetary Science Letters 271, 267–277.
Stewart, J.W., Evernden, J.F., Snelling, N.J., 1974. Age determinations from Andean Peru: a reconnaissance survey. Geological Society of America Bulletin 85, 1107–1116.
Tatsumi, T., Eggins, S., 1995. Subduction Zone Magmatism. Wiley-Blackwell.
Tera, F., Wasserburg, G.J., 1972. U–Th–Pb systematics in three Apollo 14 basalts and the problem of initial Pb in lunar rocks. Earth and Planetary Science Letters 14, 281–304.
Tiepolo, M., 2003. In situ Pb geochronology of zircon with laser ablation-inductively coupled plasma-sector field mass spectrometry. Chemical Geology 199, 159–177.
Vervoort, J.D., Blichert-Toft, J., 1999. Evolution of the depleted mantle: Hf isotope evidence from juvenile rocks through time. Geochimica et Cosmochimica Acta 63, 533–556.
Vigneresse, J.L., 2008. Granitic batholiths: from pervasive and continuous melting in the lower crust to discontinuous and spaced plutonism in the upper crust. Transactions of the Royal Society of Edinburgh: Earth Sciences 97, 311–324.
Walker Jr., B.A., Miller, C.F., Lowery Claiborne, L., Wooden, J.L., Miller, J.S., 2007. Geology and geochronology of the Spirit Mountain batholith, southern Nevada: implications for timescales and physical processes of batholith construction. Journal of Volcanology and Geothermal Research 167, 239–262.
White, S.M., Crisp, J.A., Spera, F.J., 2006. Long-term volumetric eruption rates and magma budgets. Geochemistry, Geophysics, Geosystems 7, Q03010.
Yang, J.-H., Wu, F.-Y., Wilde, S., Xie, L.-W., Yang, Y.-H., Liu, X.-M., 2007. Tracing magma mixing in granite genesis: in situ U–Pb dating and Hf-isotope analysis of zircons. Contributions to Mineralogy and Petrology 153, 177–190.